ChemComm

COMMUNICATION

Selective Anion Sensing in High Salt Water via a Remote Indicator Displacement Assay

Received 00th January 20xx,
Accepted 00th January 20xx

DOI: 10.1039/x0xx00000x

www.rsc.org/

Briana L. Hickey,[a] Alexie Andrea P. Raz,[a] Junyi Chen,[b] Jose L. Moreno Jr.,[a] Joshua D. Hartman,[a] Wenwan Zhong,[a,b] and Richard J. Hooley[a,b]*

Water-soluble deep cavitands with cationic functions at the lower rim can selectively bind iodide anions in purely aqueous solution. By pairing this lower rim recognition with an indicator dye that is bound in the host cavity, optical sensing of anions is possible. The selectivity for iodide is high enough that micromolar concentrations of iodide can be detected in the presence of molar chloride. Iodide binding at the "remote" lower rim causes a conformational change in the host, displacing the bound dye from the cavity and effecting a fluorescence response. The sensing is sensitive, selective, and works in complex environments, so will be important for optical anion detection in biorelevant media.

Macrocyclic cavity-containing hosts have been exploited for a variety of applications in molecular recognition and sensing.[1] Examples of these hosts include calixarenes, cucurbit[n]urils, cyclophanes, and self-folding cavitands,[2] and their defined cavities allow the selective recognition of small molecule targets.[3] This recognition can often be paired with an optical reporter in an indicator displacement assay,[4] allowing sensing. This recognition is well-suited for function in aqueous solution, and can even be extended to more complex environments such as high salt buffer, urine, saliva, serum, lipid membranes and living cells.[5] Anions are less commonly recognized by this type of cavity-containing host, however. The cavities of macrocyclic aromatic hosts are generally electron-rich, and favour the recognition of cations or hydrophobic molecules.[3] Gibb has shown that anion recognition in aromatic cavity-containing molecules is driven by favourable water expulsion from the cavity, modulated by Hofmeister effects.[6] Other anion-binding macrocycles[7] exploit directed hydrogen bonding groups[8] such as ureas[9] or electron poor C-H bonds[10] to bind anions. The greatest affinity and selectivity is seen with rigid macrocyclic species that provide optimal cavities, decorated with perfectly positioned coordinating groups.[10] Flexible receptors are far less effective, especially in water, where anion desolvation penalties must be overcome. Function in pure water and high-salt buffer is complicated by the need to confer water-solubility on the receptor and achieve selectivity in the presence of competitors.

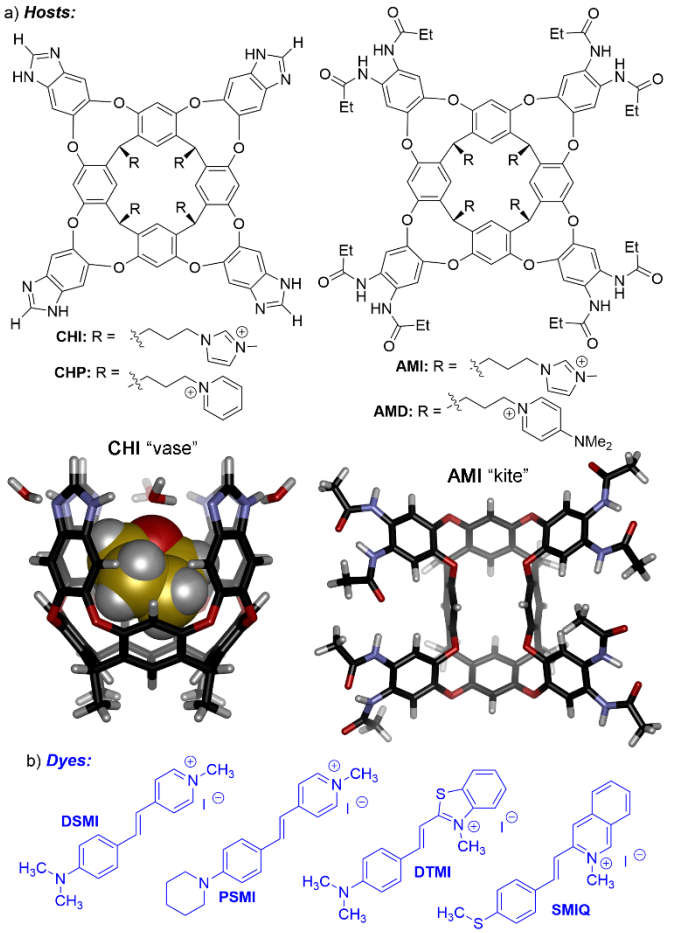

Figure 1. a) Cationic cavitands tested for anion recognition and minimized structures of the favored conformations of **CHI** (with a THF molecule in the cavity, side view) and **AMI** (top view) in solution (lower rim groups truncated for clarity, SPARTAN, AM1 forcefield), and b) dyes used for indicator displacement sensing.

[a]*Department of Chemistry;* [b]*Environmental Toxicology Graduate Program; University of California–Riverside, Riverside, CA 92521, U.S.A. *E-mail: richard.hooley@ucr.edu*

† Electronic Supplementary Information (ESI) available: Experimental methods, and fluorescence, NMR and isothermal calorimetry data not shown in the text. See DOI: 10.1039/x0xx00000x

We have recently shown that cationic, flexible, self-folding deep cavitands such as **AMI**, **CHI**, **CHP** or **AMD** (Figure 1) have affinity for complex polyanions such as DNA G-quadruplexes.[11] These hosts are quite unusual anion receptors, in that they are flexible and display electron-rich cavities. Gibb has shown that smaller, rigid cavitands can bind anions in water at the lower rim "crown", in close proximity with cationic R-NMe_3^+ ions.[12] This recognition mechanism introduces another possibility: using the bowl-shaped cavity to bind an indicator molecule, then exploiting lower rim anion binding to cause a change in fluorescence response and allowing *optical* detection of anions. Here we show that cationic, flexible self-folding deep cavitands can selectively bind anions in water and high-salt buffer, and can be used for selective optical anion sensing.

Four different cationic hosts were tested (Figure 1a). The two benzimidazole cavitands **CHP** and **CHI** are kinetically stable in water, held in the "vase" conformation by intercalated water, whereas cavitands **AMI** and **AMD** exist as the open "kite" form[13] in the absence of a cavity-filling guest. These cavitands were paired with a series of styrylpyridinium dyes, **DSMI**, **PSMI**, **DTMI** and **SMIQ** (Figure 1b). These cationic dyes bind in the host cavities, causing a reorganization of the flexible amide cavitands into the vase conformation, and show an increase in emission once bound.[11]

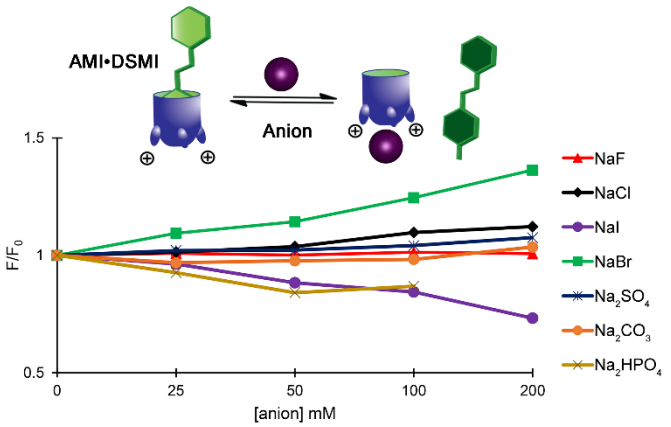

Figure 2. Fluorescence responses obtained by the titration of different anions into a solution of **AMI** host (5 µM) and **DSMI** dye (5 µM) in 20 mM Tris buffer, pH 7.4. F_0 = emission of host•dye complex in the absence of anion.

The initial sensing tests were performed in Tris buffer to avoid any competition with anions in other buffered solutions. The host:dye complexes (5 µM each) were dissolved in 20 mM Tris, pH 7.4, titrated with increasing concentrations of a variety of anions (0-200 mM), and the change in emission was measured. The fluorescence (F/F_0) plots are shown in Figure 2 (for the **AMI/DSMI** pair) and ESI Figures S1 – S7 (all other combinations). Despite the similarity in structure of the hosts and dyes, the fluorescence changes in the presence of anion were quite variable. By far the greatest changes in emission were seen with **AMI/DSMI** (Figure 2). Anions such as F^-, Cl^-, SO_4^{2-} or CO_3^{2-} caused minimal change in emission, even at 200 mM, but I^- and HPO_4^{2-} effected a significant drop in emission and Br^- caused an *increase* in emission.

Changing the dye to either **DTMI** or **SMIQ** (5 µM again) resulted in a much smaller change in F/F_0, and only I^- caused any significant change (Figure S4). Notably, none of the dyes showed appreciable loss of fluorescence in the presence of anions by themselves. When the benzimidazole cavitands **CHI** and **CHP** were used, the broad trends were similar to those shown by amide cavitand **AMI** (Figures S5, S6): iodide causes the greatest drop in fluorescence, but the magnitude of the decrease was lower than with **AMI**. More specifically, **CHI/DSMI** only showed appreciable fluorescence decrease with iodide, and then only 18% lowering after 200 mM anion addition. **CHP/DSMI** showed identical behavior with iodide, but was also mildly sensitive to carbonate and bromide. This suggests that the flexible amide cavitand scaffold is more responsive to anions than the kinetically stable benzimidazole scaffold.

We investigated the halide binding properties of **AMI** in more detail, using ITC and NMR analysis (Figure 3 and S15-S17, S20). Isothermal calorimetry was performed by adding solutions of NaCl, NaBr and NaI into a 1 mM solution of **AMI** in ultrapure water. These measurements corroborated those seen with fluorescence displacement, in that I^- bound strongly to the cavitand (K_a = 4.5 x 10^3 M^{-1}), whereas Br^- bound with a much lower affinity (K_a = 381 M^{-1}) and Cl^- showed no measurable affinity. ^{1}H NMR analysis provided clues as to *where* the guests bound, as can be seen in Figure 3a. Again, titration of both NaI and NaBr to 1 mM **AMI** caused changes in some peaks in the NMR spectrum. Anion exchange was fast on the NMR timescale, and peak shifts reached saturation with NaI after addition of 5 mM guest. Saturation was not observed with NaBr, and no binding could be seen with NaCl. The shifted peaks correspond to protons on the lower rim "crown" of the cavitand, and the folding state of the host is unchanged.

The lower rim binding mode was indirectly corroborated by the DMAP-footed **AMD** cavitand. When **AMD** was exposed to I^- (and to a lesser extent, Br^-) in an NMR sample in D_2O (see Figure S18), precipitation of the host was observed, and the only signals present in the solution were those of DMAP. **AMD** binds iodide in water in a similar manner to **AMI**, accelerating the nucleophilic substitution of the cationic $DMAP^+$ groups by iodide, forming the insoluble iodo-cavitand and DMAP. When this reaction was repeated with n-butyl-dimethylamino-pyridinium iodide and NaI in D_2O (see Figure S19), no reaction was observed: molecular recognition is required for reaction.

The minimized structures of the **AMI**•I^- and **AMI**•Cl^- complexes were determined by DFT analysis (r2SCAN-D3(BJ)/def2-SVP,[14] Figure 3c,d). Aqueous solvent effects were accounted for with the polarizable continuum model CPCM. The structures show the halide ions binding at the cavitand crown with two imidazolium ions surrounding the anion: in solution, rapid exchange between the coordinating imidazolium ions would occur. The optimized structures provide some explanation for the iodide selectivity over chloride, in that the bound iodide more fully fills the "cavity" has closer contacts with the lower rim imidazolium groups than a bound chloride. It is most likely that the selectivity is driven by anion dehydration: chloride has a much larger desolvation energy in water than iodide,[15] so binding the smaller anion has a greater desolvation penalty.[12a]

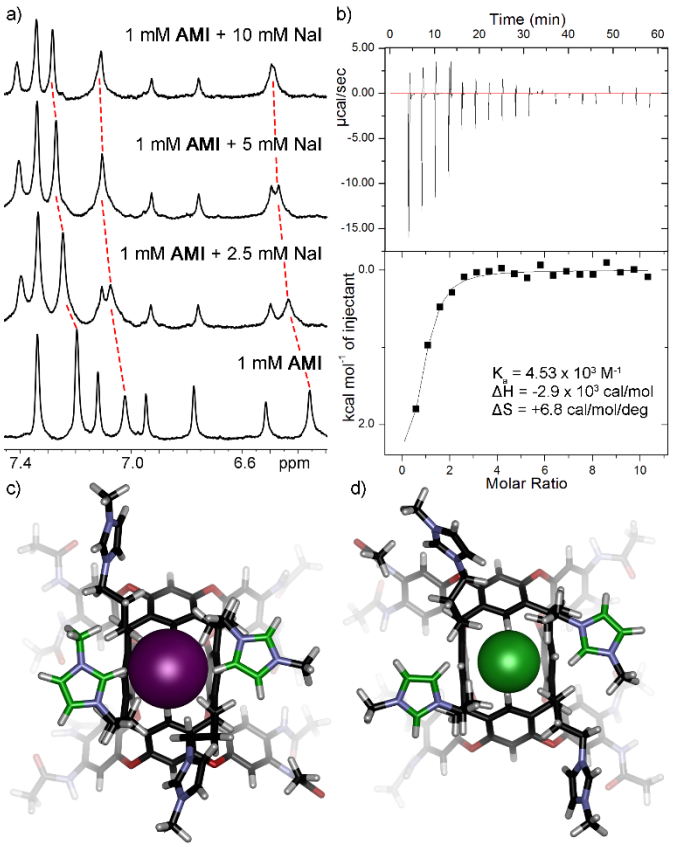

Figure 3. a) Downfield region of the ^{1}H NMR spectra of **AMI** (1 mM) in the presence of increasing amounts of added NaI (D_2O, 600 MHz, 298 K); b) ITC isotherm obtained from the addition of NaI to a 1 mM solution of **AMI** in ultrapure water. DFT-optimized structures of c) **AMI•I**$^-$; d) **AMI•Cl**$^-$ (r2SCAN-D3(BJ)/def2-SVP) viewed from the top.

We next tested the host:dye combinations for indicator displacement sensing in different media, namely in ultrapure water and 10X PBS buffer (which contains 1.4 M chloride, 80 mM NaH_2PO_4 and 20 mM KH_2PO_4). The scope was narrowed to the imidazolium hosts **AMI** and **CHI**, **DSMI** and **PSMI** dyes, and the anion scope was narrowed to the targets that effected the largest fluorescence changes in the initial screen, namely NaI, NaBr and NaH_2PO_4. The most relevant fluorescence plots are shown in Figure 4; for full plots, see Figures S8-S13.

Changing the solvent conditions from Tris buffer to ultrapure water had minimal effect on the sensing (Figure 4a). The magnitude of the changes varied slightly (iodide sensing was more effective in Tris, for example), but the overall trend was only minimally affected. In contrast, using 10X PBS buffer caused significant differences, notably a far more rapid fluorescence decrease of the **AMI-DSMI** combination in the presence of iodide, and no change in the presence of bromide (Figure 4b). The changes are notable: increasing the I$^-$ concentration from 0 mM to 200 mM in water or 20 mM Tris caused a slow, linear reduction in fluorescence with no observed saturation (Figure 2). In contrast, when the titration was repeated in 10X PBS buffer, a rapid drop in fluorescence from 0 to 25 mM I$^-$ was observed, followed by minimal change with increased anion concentration (Figure 4b). This suggests that the presence of phosphate and chloride in the solution *enhances* the sensing capabilities for iodide. To this end, the limit of detection was calculated (see Figure S-21), and LOD (I$^-$) = 21 µM in 10X PBS buffer was observed. The conformational preferences of the cavitand influence the fluorescence response: when **CHI** was used, which has identical lower rim groups but favors a folded vase conformation in solution, the fluorescence was similar to that observed in water (Figure 4c).

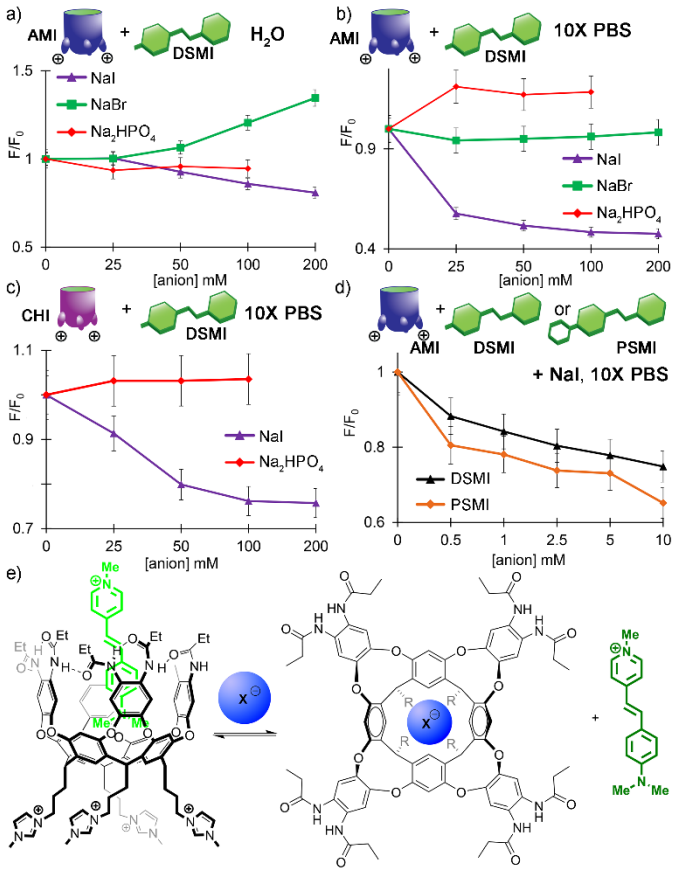

Figure 4. Fluorescence responses obtained by the titration of different anions into cavitand:dye solutions: a) **AMI** (5 µM), **DSMI** (5 µM) in ultrapure water; b) **AMI** (5 µM), **DSMI** (5 µM) in 10X PBS buffer (1.37 M NaCl, 27 mM KCl, 80 mM NaH_2PO_4 and 20 mM KH_2PO_4); c) **CHI** (5 µM), **DSMI** (5 µM) in 10X PBS buffer; d) titration of NaI into a solution of **AMI** (5 µM) and either **DSMI** (5 µM) or **PSMI** (5 µM) in 10X PBS buffer. pH = 7.4. e) Mechanism of iodide sensing with the **AMI** cavitand: a conformational switch occurs upon iodide binding, opening the host and disfavoring **DSMI** binding.

These observations introduce mechanistic questions: Why does I- binding at the cavitand base cause a decrease in observed fluorescence, and why is the sensing performance of **AMI** so much greater than **CHI**, when the recognition unit at the lower rim of the host is unchanged? Also, why does Br$^-$ binding cause an increase in emission, but only with the **AMI** cavitand and only in water or Tris buffer?

The most plausible theory for the iodide sensing selectivity is illustrated in Figure 4e: in the absence of guest, **AMI** exists in the unfolded "kite" conformation, which deforms the cavitand and the lower rim functional groups. When a dye is bound in the cavity, it adopts a folded "vase" conformation, which should have less flexibility for the lower rim groups to bind anions. Therefore, binding iodide at the base should favor a reorganization of the cavitand, *disfavouring* dye binding and

causing a drop in emission. To support this theory, we established the relative affinity of the dye for **AMI** in ultrapure water, as well in the presence of 50 mM NaBr or 50 mM NaI *via* fluorescence emission titrations. Hill 1 plot analysis of the titration curves shows that the affinity of **DSMI** for **AMI** in ultrapure water is (K_d = 17 μM), whereas in the presence of 50 mM NaI, the affinity drops to K_d = 60 μM. This corroborates the proposed sensing mechanism: in the presence of coordinating iodide salts, the reorganization at the cavitand base disfavors guest binding, expunging the dye and lowering the emission.

Further evidence can be seen by varying the bound dye. The **DSMI** dye binds in the cavity of **AMI**, but it shows a rapid in/out exchange with no discrete Michaelis complex, just averaged peak shifts between the two observed populations in the ^{1}H NMR spectrum.[16] In contrast, the larger **PSMI** dye shows slow exchange and clear free/bound host peaks, (Figure S-19). As can be seen in Figure 4d, the **AMI/PSMI** complex shows a larger decrease in fluorescence upon iodide addition than **AMI/DSMI**: in this case, the conformational switch is more pronounced, causing a greater difference in dye affinity.

The Hill plot analysis also provides some insight into why the emission of **AMI/DSMI** *increases* upon addition with NaBr (Figure 2), a property not seen with other combinations of anion, host and dye. In the presence of bromide (and only bromide), the Hill plot of **AMI/DSMI** fluorescence response is sigmoidal (Figure S-22), indicating that multiple binding modes of **DSMI** are present. The binding affinity of **DSMI** in the presence of 50 mM NaBr (K_d = 31 μM) is lower than that in pure water, but higher than with 50 mM NaI, and while the Hill Plot fitting was not perfect, evidence for n>1 binding is seen. Water-soluble self-folding cavitands are well-precedented to undergo aggregation in salt solution,[16] so it is likely that hydrophobic aggregates of **AMI** and **DSMI** are present in solution, and the presence of salts (especially bromide) cause formation of aggregates that increase **DSMI** fluorescence. This observation is speculative, but is also likely linked to the fact that that the sensing of iodide is more effective in the presence of high salt concentrations. Gibb has elegantly shown that the affinities of halide ions to rigid cationic hosts are attenuated in the presence of phosphate due to competitive buffer complexation.[15a] In our case, the low LOD of iodide ions in 10X PBS buffer is not due to enhanced affinity for iodide in high salt, but a greater change in fluorescence response from the **AMI/DSMI** host:guest complex. By pairing multiple recognition motifs for sensing anions, multiple mechanisms can be exploited to enhance the response that are not solely dependent on binding affinity.

In conclusion, we have shown that flexible, water-soluble deep cavitands with cationic imidazolium functions at the lower rim can bind anions in purely aqueous solution. By pairing this lower rim recognition with an indicator dye bound in the host cavity, the molecular recognition process can be converted to an optical sensing platform, whereby micromolar concentrations of iodide (LOD = 21 μM) can be detected in 10X PBS buffer. The sensing is most effective when a flexible cavitand is used, as iodide binding at the remote lower rim causes a conformational change in the host, displacing the bound dye from the cavity and effecting the greatest fluorescence response.

The authors thank the National Science Foundation (CHE-2002619 to R.J.H. and CHE-1707347 to W.Z.), for support.

Conflicts of interest

There are no conflicts to declare.

Notes and references

1 (*a*) R. Pinalli, A. Pedrini, E. Dalcanale, *Chem. Soc. Rev.* 2018, **47**, 7006; (*b*) S. van Dun, C. Ottmann, C.; L.-G. Milroy and L. Brunsveld, *J. Am. Chem. Soc.* 2017, **139**, 13960.

2 (*a*) C.-L. Deng, S. L. Murkli and L. D. Isaacs, *Chem. Soc. Rev.*, 2020, **49**, 7516; (*b*) J. Beaver and M. L. Waters, *ACS Chem. Biol.* 2016, **11**, 643; (*c*) D.-S. Guo, V. D. Uzunova, X. Su, Y. Liu and W. M. Nau, *Chem. Sci.*, 2011, **2**, 1722.

3 (*a*) Z. Laughrey and B. C. Gibb, *Chem. Soc. Rev.*, 2011, **40**, 363; (*b*) J. H. Jordan and B. C. Gibb, *Chem. Soc. Rev.* 2015, **44**, 547; (*c*) E. E. Harrison, B. A. Carpenter, L. E. St. Louis, A. G. Mullins and M. L. Waters, *J. Am. Chem. Soc.*, 2021, **143**, 14845; (*d*) M. A. Beatty, J. Borges-González, N. J. Sinclair, A. T. Pye and F. Hof, *J. Am. Chem. Soc.* 2018, **140**, 3500.

4 A. C. Sedgwick, J. T. Brewster, T. Wu, X. Feng, S. D. Bull, X. Qian, J. L. Sessler, T. D. James, E. V. Anslyn and X. Sun, *Chem. Soc. Rev.* 2021, **50**, 9.

5 (*a*) M. A. Beatty and F. Hof, *Chem. Soc. Rev.*, 2021, **50**, 4812; (*b*) M. A. Beatty, A. J. Selinger, Y. Li, F. Hof, *J. Am. Chem. Soc.*, 2019, **141**, 16763; (*c*) C. Hu, L. Grimm, A. Prabodh, A. Baksi, A. Siennicka, P. A. Levkin, M. M. Kappes and F. Biedermann, *Chem. Sci.*, 2020, **11**, 11142; (*d*) Y. Liu, T. Minami, R. Nishiyabu, Z. Wang and P. Anzenbacher, *J. Am. Chem. Soc.*, 2013, **135**, 7705.

6 (*a*) J. H. Jordan, C. L. D. Gibb, A. Wishard, T. Pham and B. C. Gibb, *J. Am. Chem. Soc.* 2018, **140**, 4092; (*b*) P. Sokkalingam, J. Shraberg, S. W. Rick and B. C. Gibb, *J. Am. Chem. Soc.*, 2016, **138**, 48; (*c*) C. L. D. Gibb, and B. C. Gibb, *J. Am. Chem. Soc.*, 2011, **133**, 7344.

7 S. J. Edwards, H. Valkenier, N. Busschaert, P. A. Gale and A. P. Davis, *Angew. Chem.*, 2015, **127**, 4675.

8 (*a*) S. Butler and K. Jolliffe, *ChemPlusChem*, 2021, **86**, 59; (*b*) S. N. Berry, L. Qin, W. Lewis and K. A. Jolliffe, *Chem. Sci.*, 2020, **11**, 7015.

9 (*a*) X. Wu and P. A. Gale, *Chem. Comm.*, 2021, **57**, 3979; (*b*) A. Borissov, I. Marques, J. Y. C. Lim, V. Félix, M. D. Smith and P. D. Beer, *J. Am. Chem. Soc.*, 2019, **141**, 4119; (*c*) A. Docker, Y. C. Tse, H. M. Tay, A. J. Taylor, Z. Zhang and P. D. Beer, *Angew. Chem. Int. Ed.*, 2022, **61**, e2022145; (*d*) A. Docker, I. Marques, H. Kuhn, Z. Zhang, V. Félix and P. D. Beer, *J. Am. Chem. Soc.*, 2022, **144**, 14778.

10 (*a*) F. C. Parks, E. G. Sheetz, S. R. Stutsman, A. Lutolli, S. Debnath, K. Raghavachari and A. H. Flood, *J. Am. Chem. Soc.*, 2022, **144**, 1274; (*b*) Y. Liu, W. Zhao, C.-H. Chen and A. H. Flood, *Science*, 2019, **365**, 159.

11 W. Zhong and R. J. Hooley, *Acc. Chem. Res.* 2022, **55**, 1035.

12 (*a*) J. H. Jordan, H. S. Ashbaugh, J. T. Mague and B. C. Gibb, *J. Am. Chem. Soc.*, 2021, **143**, 18605; (*b*) H. R. Aziz, W. Yao, J. H. Jordan and B. C. Gibb, *Supramol. Chem.*, 2021, **33**, 266.

13 J. R. Moran, J. L. Ericson, E. Dalcanale, J. A. Bryant, C. B. Knobler and D. J. Cram, *J. Am. Chem. Soc.*, 1991, **114**, 5707.

14 (*a*) J. W. Furness, A. D. Kaplan, J. Ning, J. P. Perdew and J. Sun, *J. Phys. Chem. Lett.* 2020, **11**, 8208; (*b*) A. V. Marenich, C. J. Cramer and D. G. Truhlar *J. Phys. Chem. B*, 2009, **113**, 6378.

15 K. Hiraoka, S. Mizuse and S. Yamabe, *J. Phys. Chem.* 1988, **92**, 3943.

16 A. D. Gill, B. L. Hickey, S. Wang, M. Xue, W. Zhong and R. J. Hooley, *Chem. Commun.* 2019, **55**, 13259–13262.

Selective Anion Sensing in High Salt Water via a Remote Indicator Displacement Assay

Briana L. Hickey,[a] Alexie Andrea P. Raz,[a] Junyi Chen,[b] Jose L. Moreno Jr.,[a] Joshua D. Hartman,[a] Wenwan Zhong,[a,b] and Richard J. Hooley[a,b]*

[a]*Department of Chemistry;* [b]*Environmental Toxicology Graduate Program; University of California-Riverside, Riverside, CA 92521, U.S.A.*

richard.hooley@ucr.edu

Electronic Supplementary Information

Table of Contents

General Information

Cavitands **AMI**[1], **CHI**[2], **AMD**[3] and **CHP**[2] as well as fluorescent guests **DSMI**[2], **DTMI**[3], and **2-SMIQ**[3] were synthesized and characterized according to literature procedures. Deuterated NMR solvents were obtained from Cambridge Isotope Laboratories (Andover, MA), and used without further purification. All other materials were purchased from Sigma Aldrich (St. Louis, MO) or Fisher Scientific (Fairlawn, NJ), and were used as received. NMR spectra were recorded on a Bruker Avance Neo 600 MHz NMR spectrometer. All NMR spectra were processed using MestReNova by Mestrelab. NMR experiments were done by titrating increasing volumes of a 10 mM solution of the target anion dissolved in D_2O into 300 µL of a 1 mM solution of host also dissolved in D_2O. Fluorescence measurements were performed with a Bio-Tek Synergy HT Multi-Detection Microplate Reader.

Fluorescence measurements. In general, the fluorescence assays were carried out by mixing 10 µL of the fluorescent guest (5 µM in water), 10 µL of cavitand host (5 µM in water), and 10 µL ionic salts (0-500 mM in water), then adding 70 µL of the incubation buffer (Tris buffer HCl, pH 7.4, 20 mM, ultrapure H_2O, or 10X PBS buffer) to bring the total volume up to 100 µL for each well in the 96-well plate, then incubating with mild agitation for 15 min at room temperature. Each experimental condition was repeated in quadruplicate across four separate wells of the 96-well plate using identical sensor components, simultaneously collecting fluorescence signals for each target at one time. The fluorescence signal (F) was recorded with the Ex/Em wavelengths at 485/600 nm for all fluorescent guests.

Isothermal Titration Calorimetry Measurements. All ITC experiments were performed using a MicroCal iTC200 (GE Healthcare, Freiburg, Germany) with a stirring rate of 700 rpm. The baseline was stabilized prior to the experiment, and a pre-injection delay was set to 60 s. A stock solution of **NaI**, **NaBr** or **NaCl** at 50 mM dissolved in ultrapure H_2O was added in 2 µL aliquots to the **AMI** solution of 1 mM in ultrapure H_2O, respectively. All experiments were conducted at 20 °C. The heat of dilution, measured by the injection of titrant into H_2O, was subtracted for each titration to obtain the net reaction heat value. Curve fitting was performed by the MicroCal program using the One Set of Sites model.

Computational Methods. Geometry optimizations were performed using the r^2SCAN[4] meta-generalized gradient approximation (GGA) density functional with the D3(BJ) dispersion correction[5,6] and the def2-SVP[7] basis set. Solvent effects were accounted for in the geometry optimizations using the conductor-like polarizable continuum model, CPCM, with water as the solvent.[8] Density fitting using the def2/J auxiliary basis was used to accelerate the calculation. All geometry optimizations were performed using the ORCA 5.0 software package.[9]

Fluorescence Data

Screening of Host•Dye•Anion Combinations in Tris

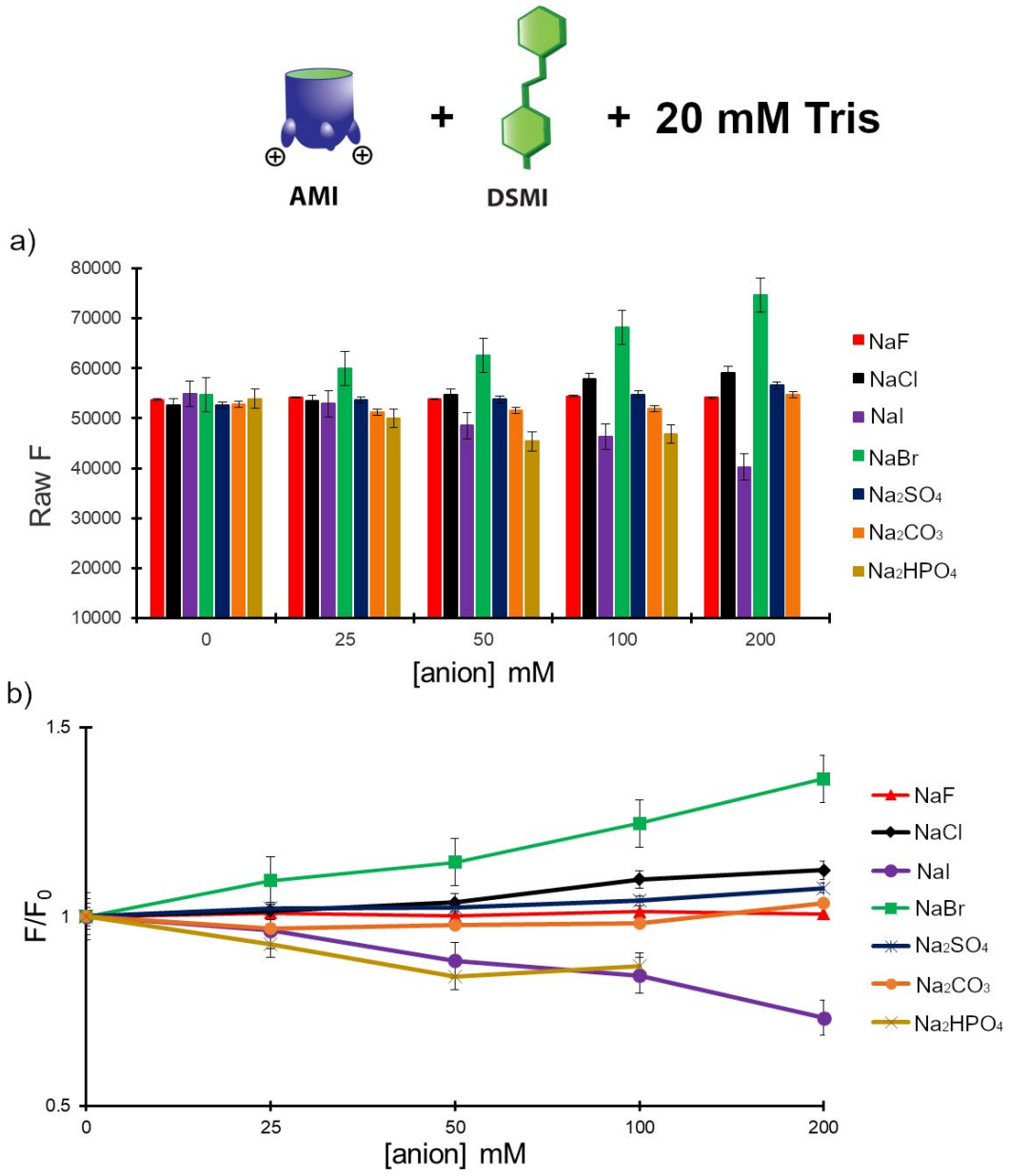

Figure S-1. Relative fluorescence responses of the **AMI•DSMI•X**$^-$ complex in 20 mM Tris buffer, pH 7.4. [**AMI**] = 5 μM, [**DSMI**] = 5 μM. F_0 = fluorescence response of the **AMI•DSMI** complex, F = fluorescence response of the **AMI•DSMI•X**$^-$ complex, where a) is the raw fluorescence of **AMI•DSMI•X** and b) is the F/F_0 response of **AMI•DSMI•X**$^-$.

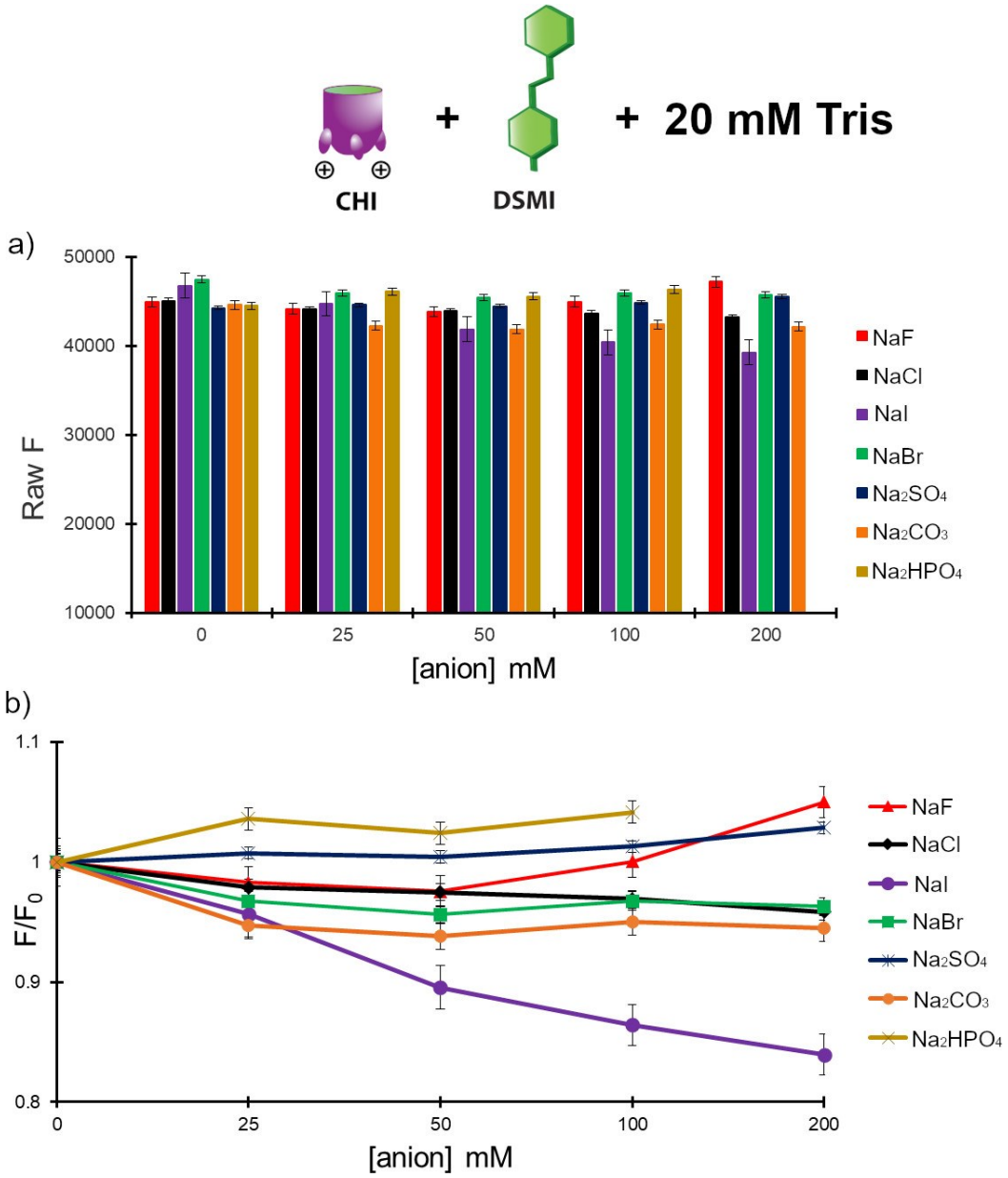

Figure S-2. Relative fluorescence responses of the **CHI•DSMI•X**$^-$ complex in 20 mM Tris buffer, pH 7.4. [**CHI**] = 5 μM, [**DSMI**] = 5 μM. F_0 = fluorescence response of the **CHI•DSMI** complex, F = fluorescence response of the **CHI•DSMI•X**$^-$ complex where, a) is the raw fluorescence of **CHI•DSMI•X**$^-$and b) is the F/F_0 response of **CHI•DSMI•X**$^-$.

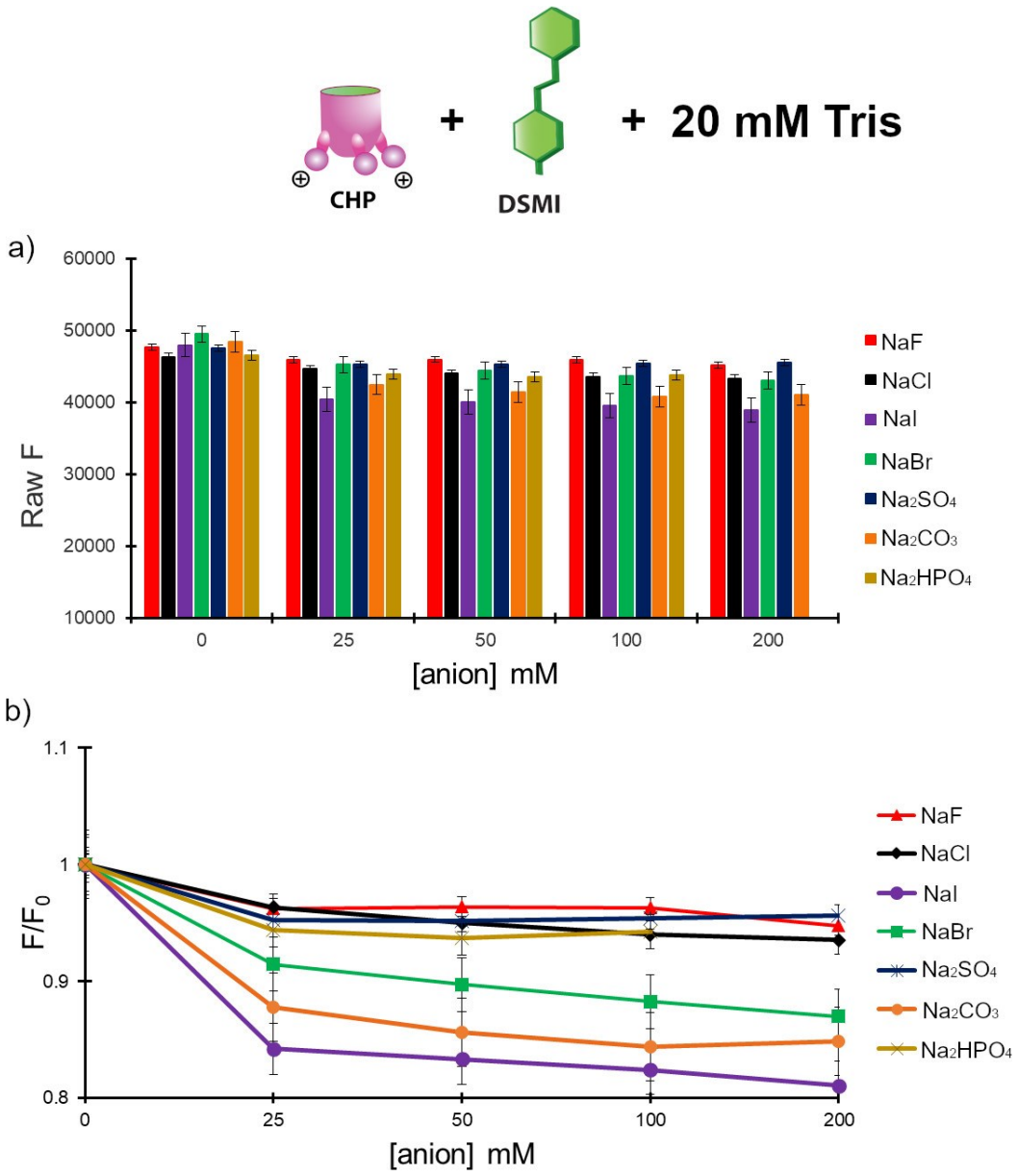

Figure S-3. Relative fluorescence responses of the **CHP•DSMI•X**$^-$ complex in 20 mM Tris buffer, pH 7.4. [**CHP**] = 5 μM, [**DSMI**] = 5 μM. F_0 = fluorescence response of the **CHP•DSMI** complex, F = fluorescence response of the **CHP•DSMI•X**$^-$ complex where, a) is the raw fluorescence of **CHP•DSMI•X**$^-$ and b) is the F/F_0 response of **CHP•DSMI•X**$^-$.

Host•Dye•Anion Combinations in Tris Buffer

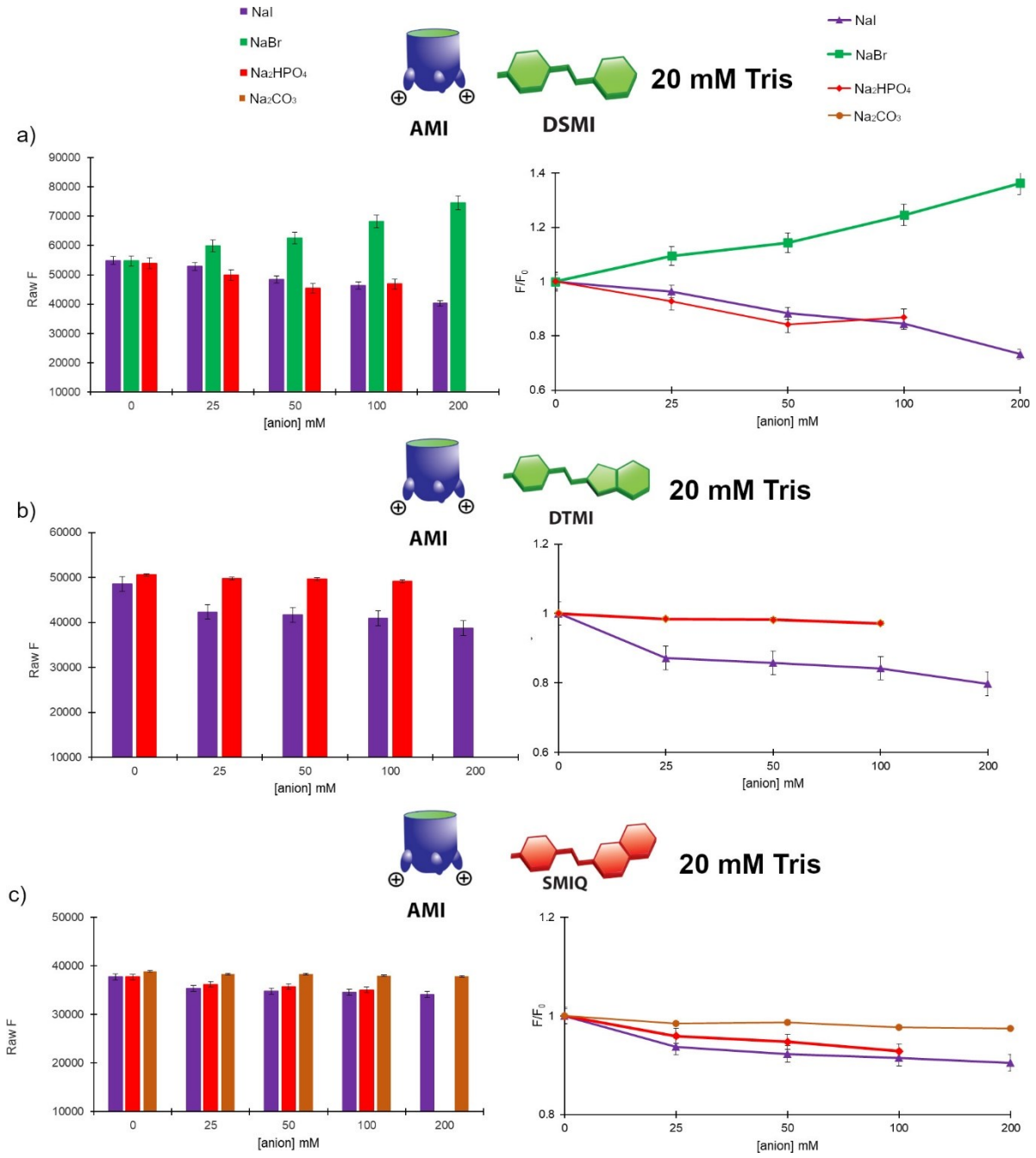

Figure S-4. Relative fluorescence responses of the **AMI•Dye•X**$^-$ complex in 20mM Tris buffer, pH 7.4, [**AMI**] = 5 μM, [**Dye**] = 5 μM. F_0 = fluorescence response of the **AMI•Dye** complex, F = fluorescence response of the **AMI•Dye•X**$^-$ complex where a) is the response of **AMI•DSMI•X**$^-$, b) is the response of **AMI•DTMI•X**$^-$, and c) is the response of **AMI•SMIQ•X**$^-$.

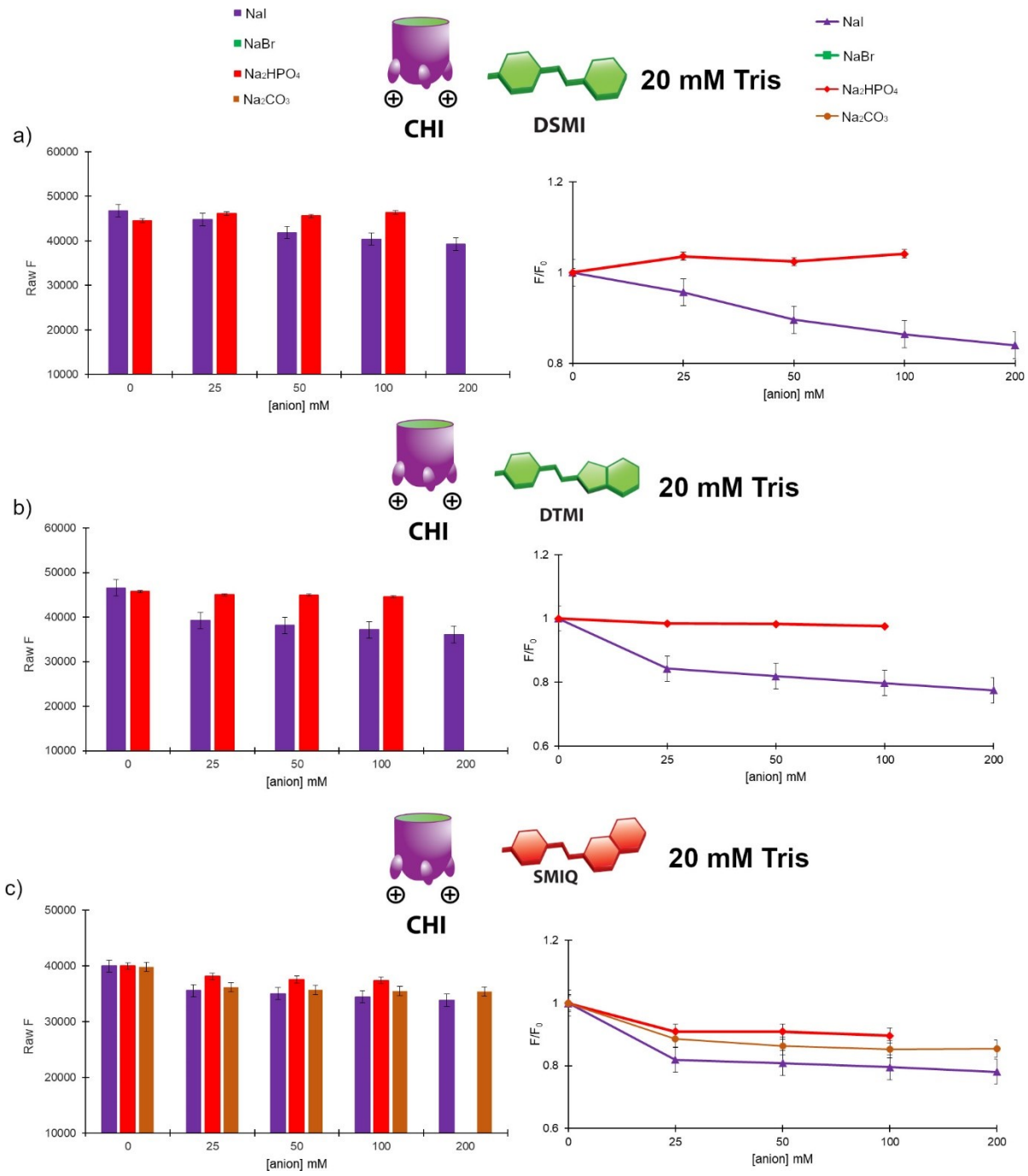

Figure S-5. Relative fluorescence responses of the **CHI•Dye•X**$^-$ complex in 20mM Tris buffer, pH 7.4, [**CHI**] = 5 μM, [**Dye**] = 5 μM. F_0 = fluorescence response of the **CHI•Dye** complex, F = fluorescence response of the **CHI•Dye•X**$^-$ complex where a) is the response of **CHI•DSMI•X**$^-$, b) is the response of **CHI•DTMI•X**$^-$, and c) is the response of **CHI•SMIQ•X**$^-$.

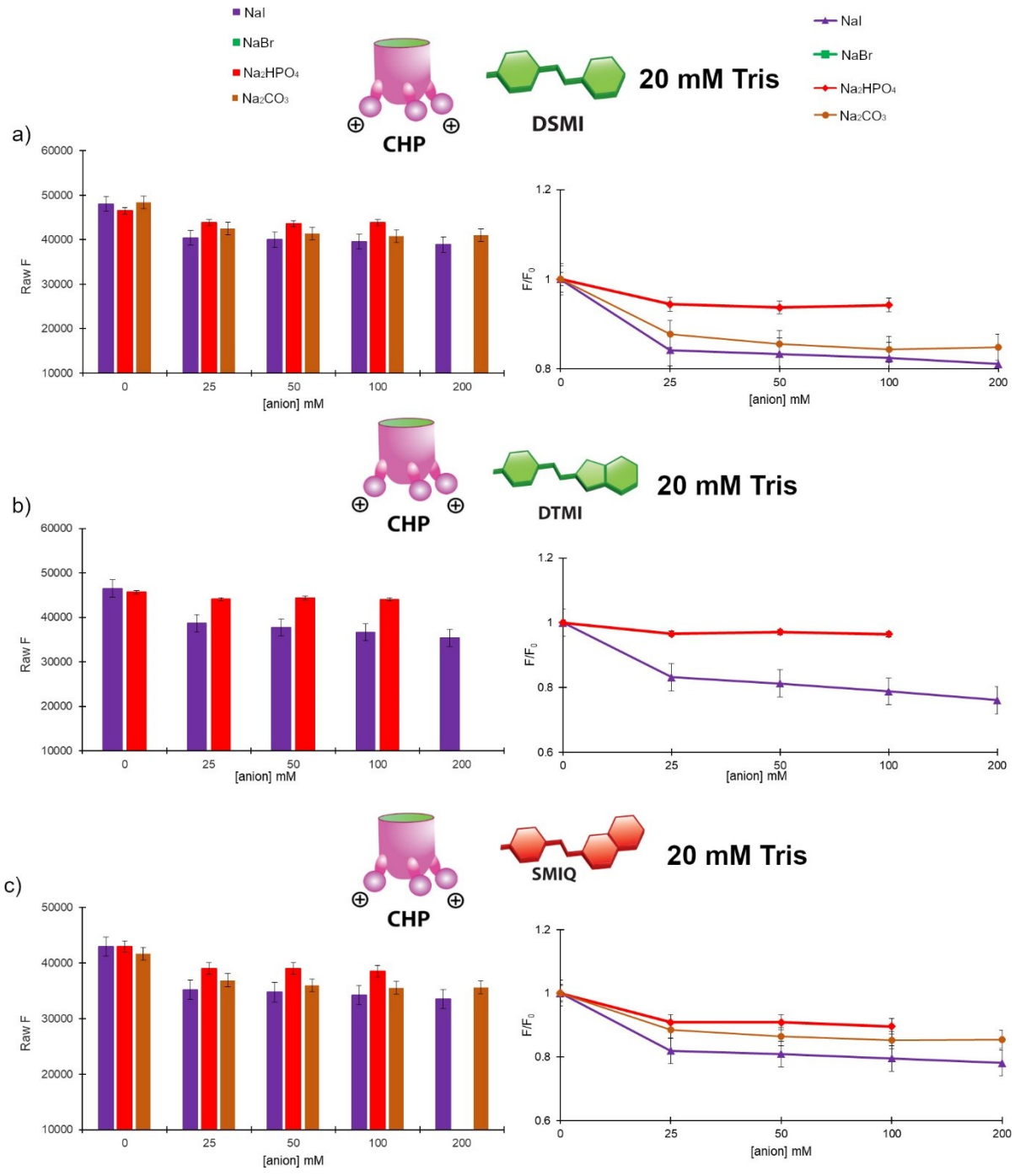

Figure S-6. Relative fluorescence responses of the **CHP•Dye•X**$^-$ complex in 20mM Tris buffer, pH 7.4, [**CHP**] = 5 μM, [**Dye**] = 5 μM. F_0 = fluorescence response of the **CHP•Dye** complex, F = fluorescence response of the **CHP•Dye•X**$^-$ complex where a) is the response of **CHP•DSMI•X**$^-$, b) is the response of **CHP•DTMI•X**$^-$, and c) is the response of **CHP•SMIQ•X**$^-$.

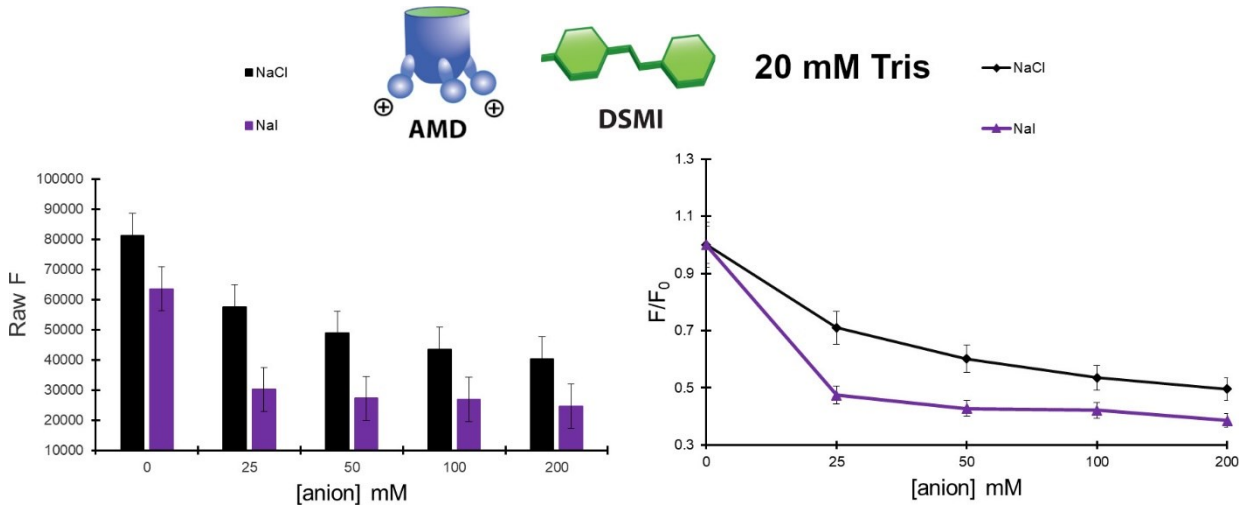

Figure S-7. Relative fluorescence responses of the **AMD•DSMI•X**$^-$ complex in 20mM Tris buffer, pH 7.4, [**AMD**] = 5 μM, [**DSMI**] = 5 μM. F_0 = fluorescence response of the **AMD•DSMI** complex, F = fluorescence response of the **AMI•DSMI•X**$^-$ complex.

Host•Dye•Anion Combinations in Ultrapure H_2O

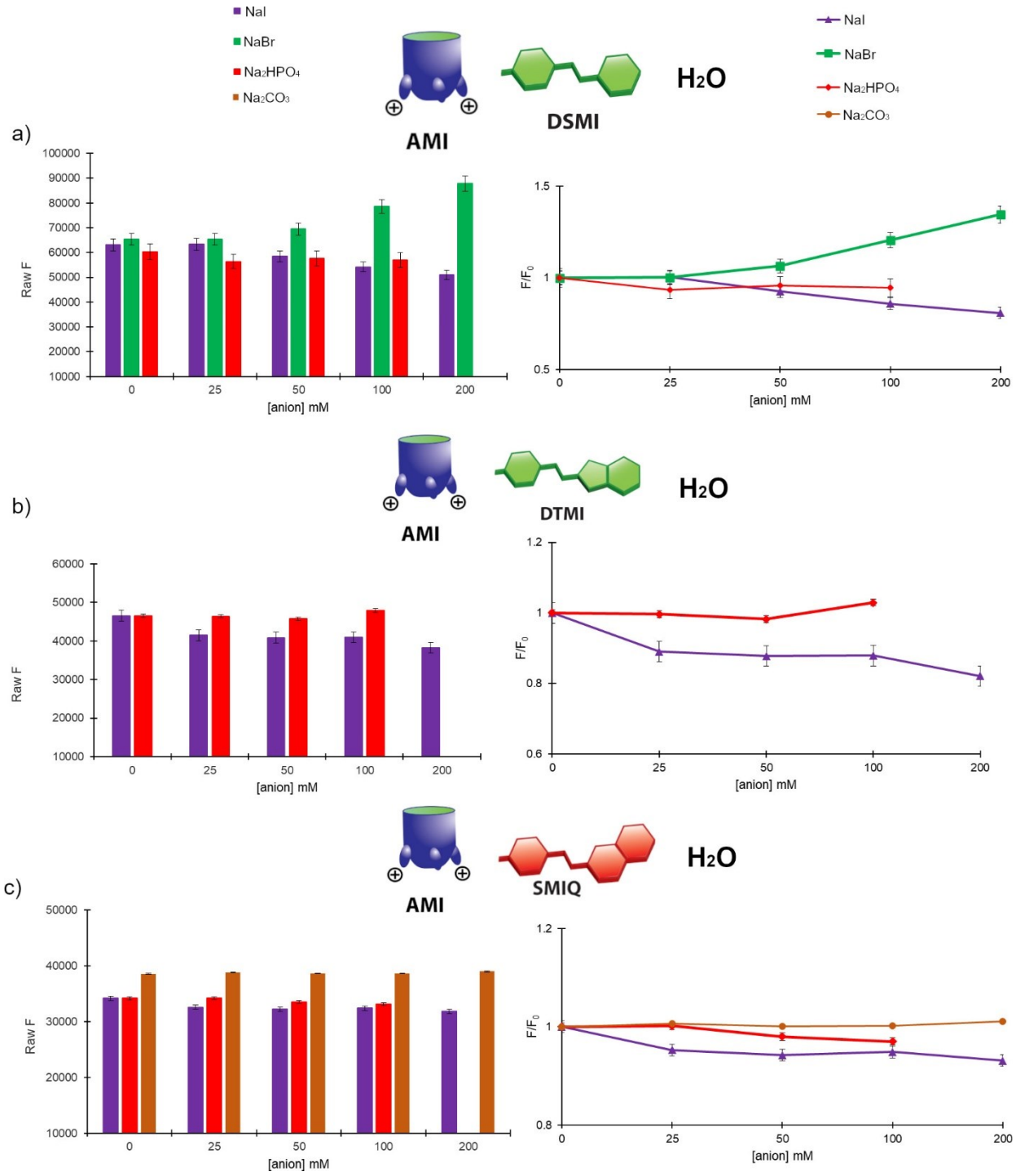

Figure S-8. Relative fluorescence responses of the **AMI•Dye•X**$^-$ complex in ultrapure H_2O, pH 7.4, [**AMI**] = 5 μM, [**Dye**] = 5 μM. F_0 = fluorescence response of the **AMI•Dye** complex, F = fluorescence response of the **AMI•Dye•X**$^-$ complex where a) is the response of **AMI•DSMI•X**$^-$, b) is the response of **AMI•DTMI•X**$^-$, and c) is the response of **AMI•SMIQ•X**$^-$.

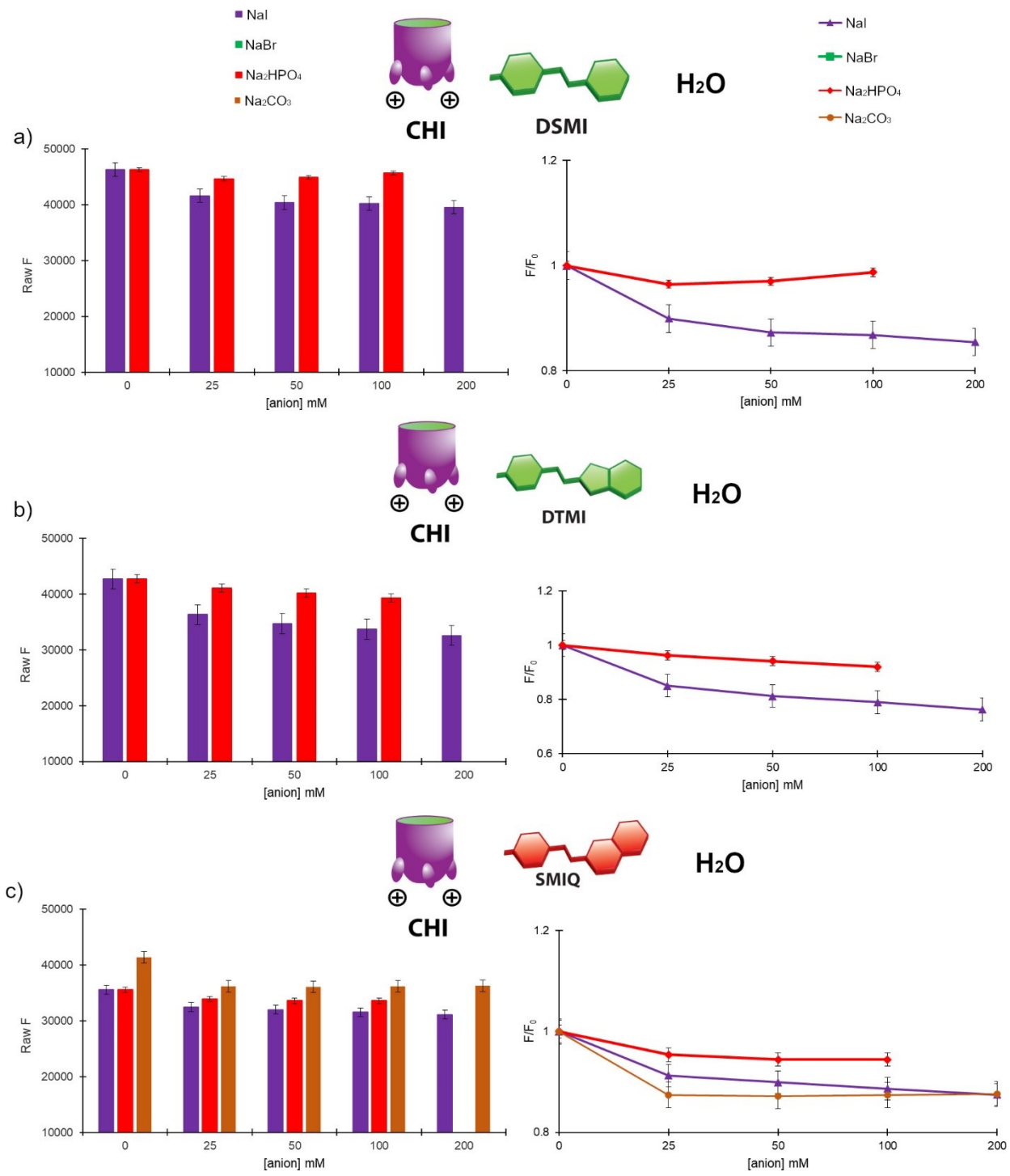

Figure S-9. Relative fluorescence responses of the **CHI•Dye•X**$^-$ complex in ultrapure H_2O, pH 7.4, [**CHI**] = 5 μM, [**Dye**] = 5 μM. F_0 = fluorescence response of the **CHI•Dye** complex, F = fluorescence response of the **CHI•Dye•X**$^-$ complex where a) is the response of **CHI•DSMI•X**$^-$, b) is the response of **CHI•DTMI•X**$^-$, and c) is the response of **CHI•SMIQ•X**$^-$.

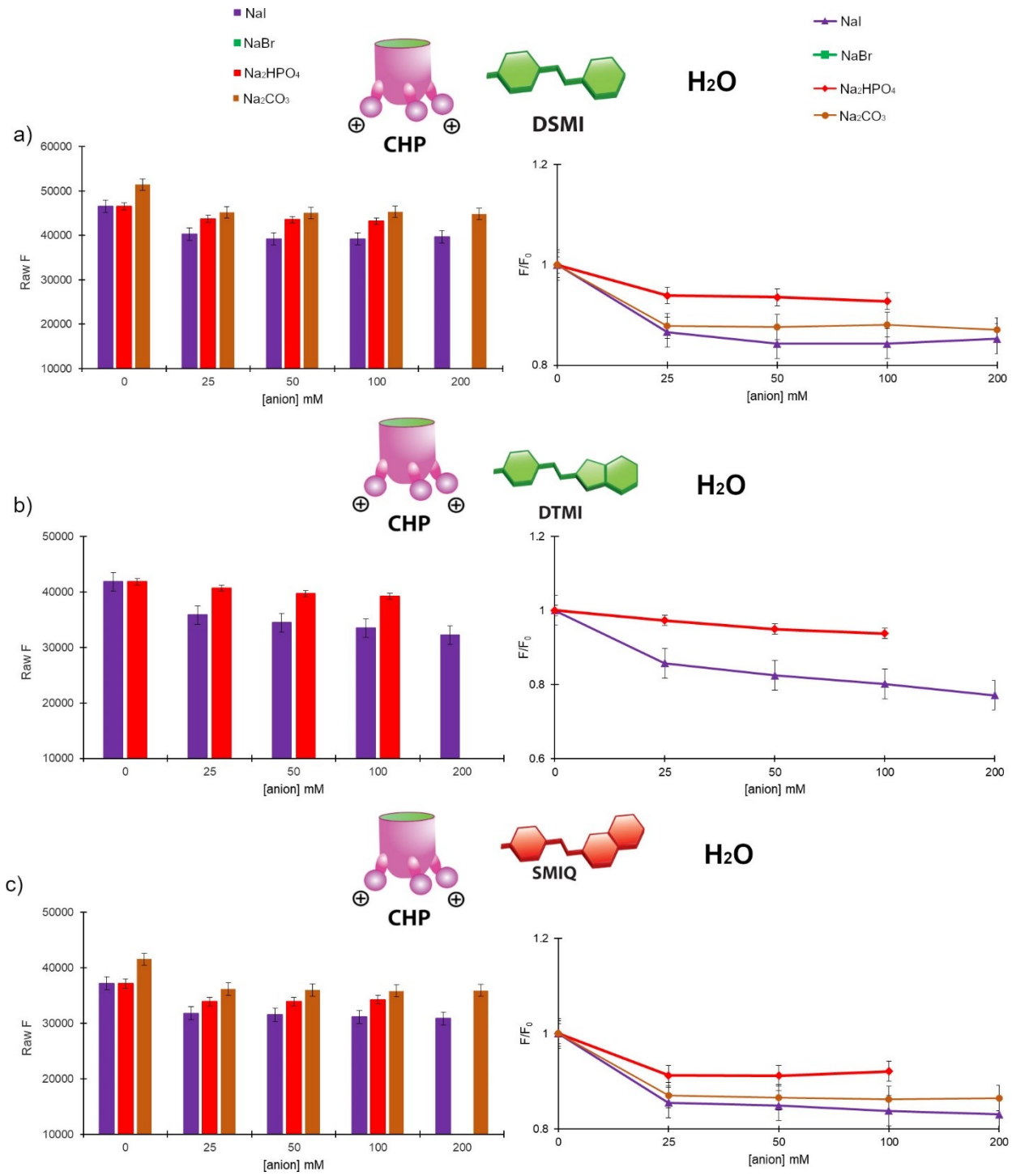

Figure S-10. Relative fluorescence responses of the **CHP•Dye•X**$^-$ complex in ultrapure H_2O, pH 7.4, [**CHP**] = 5 μM, [**Dye**] = 5 μM. F_0 = fluorescence response of the **CHP•Dye** complex, F = fluorescence response of the **CHP•Dye•X**$^-$ complex where a) is the response of **CHP•DSMI•X**$^-$, b) is the response of **CHP•DTMI•X**$^-$, and c) is the response of **CHP•SMIQ•X**$^-$.

Host•Dye•Anion Combinations in 10X PBS Buffer (1.37 M NaCl, 27 mM KCl, 80 mM NaH_2PO_4, and 20 mM KH_2PO_4)

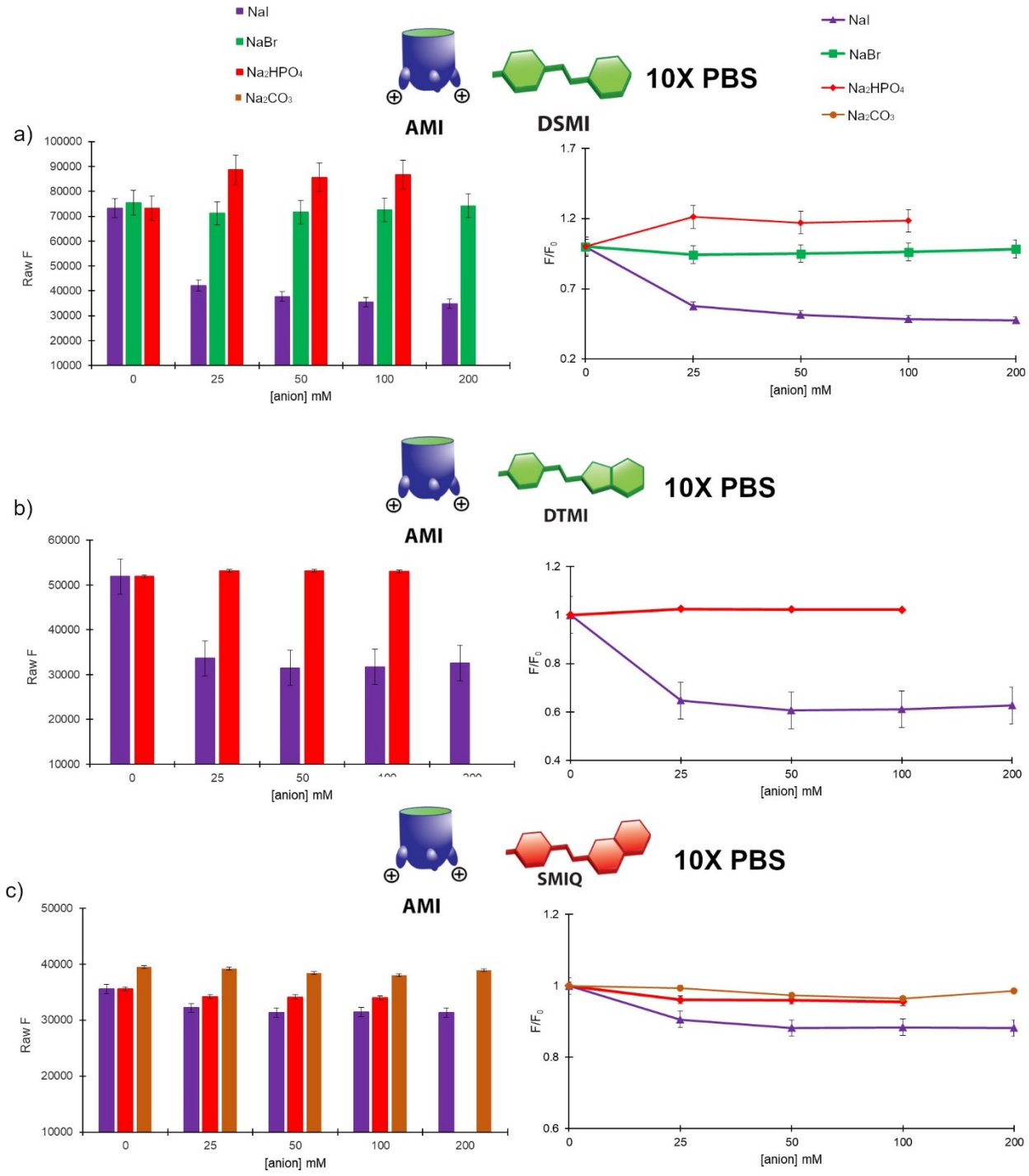

Figure S-11. Relative fluorescence responses of the **AMI•Dye•X**$^-$ complex in 10X PBS, pH 7.4, [**AMI**] = 5 μM, [**Dye**] = 5 μM. F_0 = fluorescence response of the **AMI•Dye** complex, F = fluorescence response of the **AMI•Dye•X**$^-$ complex where a) is the response of **AMI•DSMI•X**$^-$, b) is the response of **AMI•DTMI•X**$^-$, and c) is the response of **AMI•SMIQ•X**$^-$.

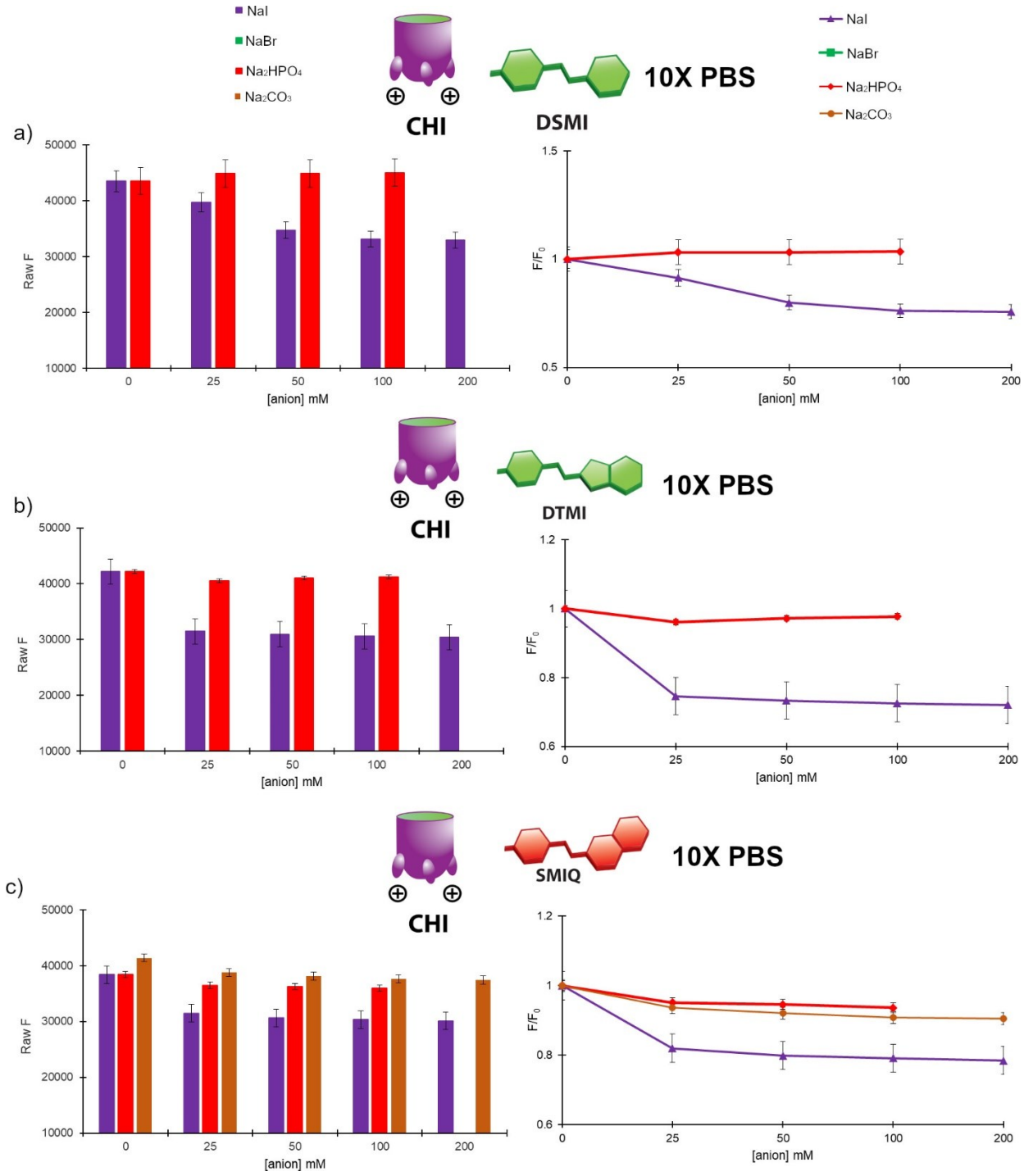

Figure S-12. Relative fluorescence responses of the **CHI•Dye•X**$^-$ complex in 10X PBS, pH 7.4, [**CHI**] = 5 μM, [**Dye**] = 5 μM. F_0 = fluorescence response of the **CHI•Dye** complex, F = fluorescence response of the **CHI•Dye•X**$^-$ complex where a) is the response of **CHI•DSMI•X**$^-$, b) is the response of **CHI•DTMI•X**$^-$, and c) is the response of **CHI•SMIQ•X**$^-$.

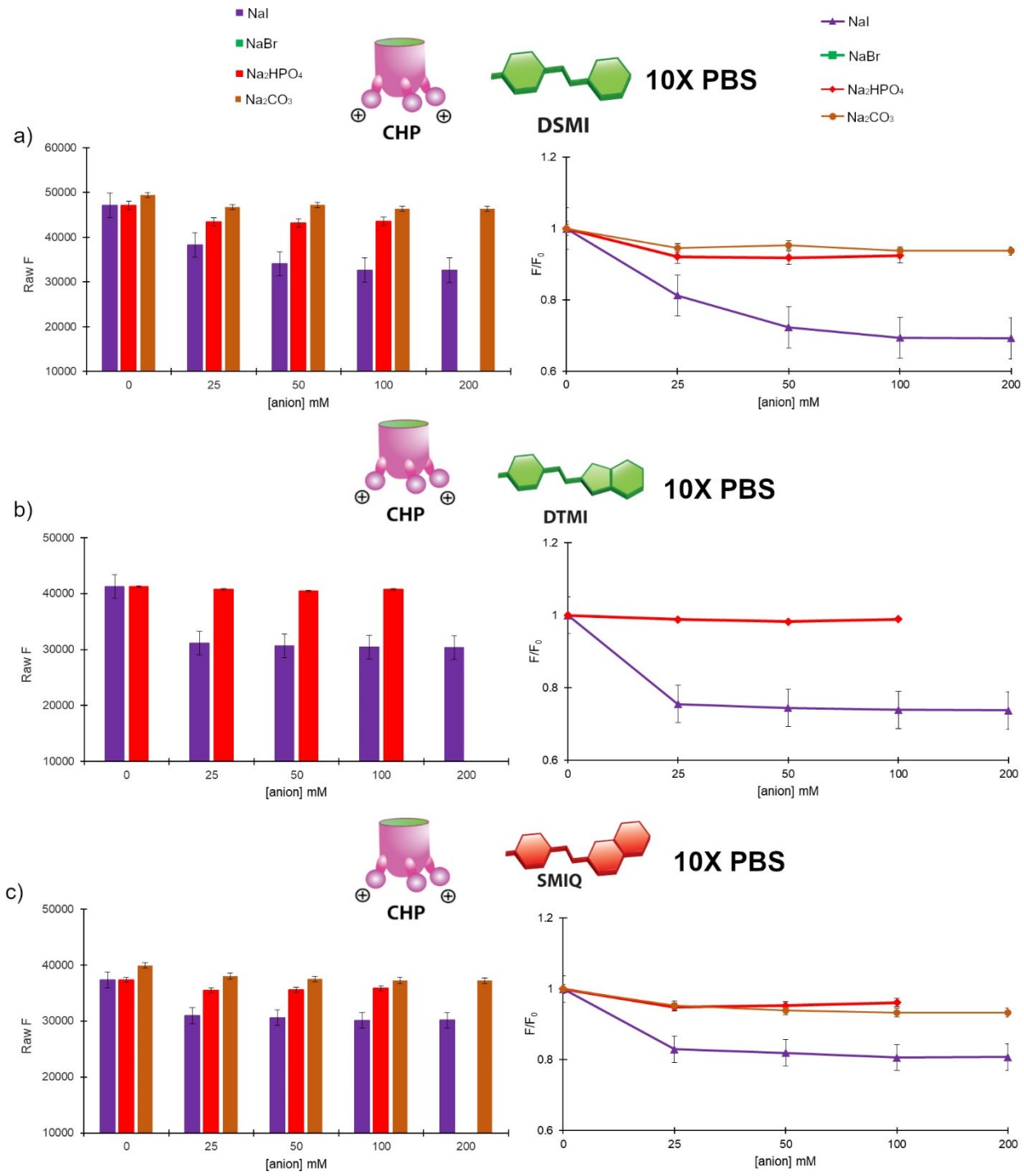

Figure S-13. Relative fluorescence responses of the **CHP•Dye•X**$^-$ complex in 10X PBS, pH 7.4, [**CHP**] = 5 μM, [**Dye**] = 5 μM. F_0 = fluorescence response of the **CHP•Dye** complex, F = fluorescence response of the **CHP•Dye•X**$^-$ complex where a) is the response of **CHP•DSMI•X**$^-$, b) is the response of **CHP•DTMI•X**$^-$, and c) is the response of **CHP•SMIQ•X**$^-$.

Controls

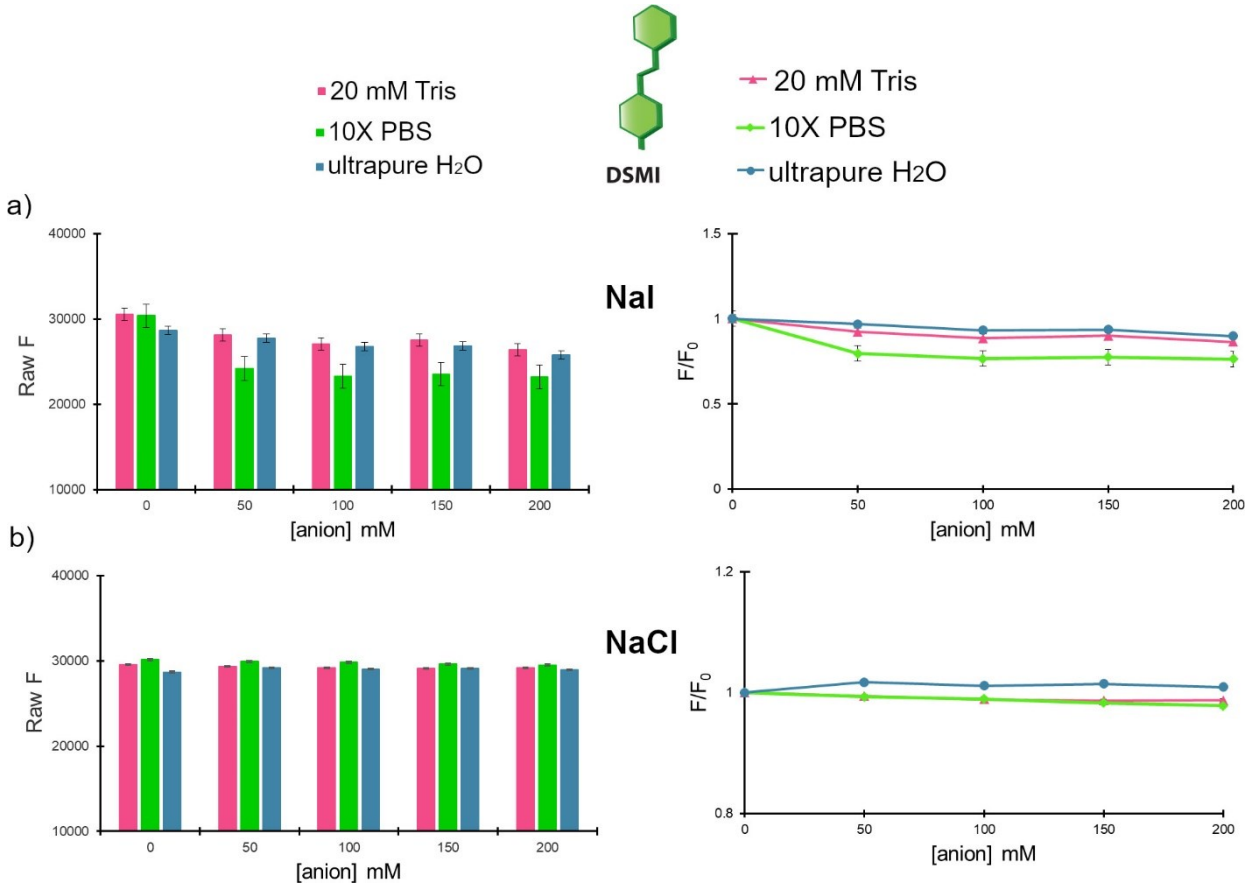

Figure S-14. Relative fluorescence responses of the **Dye•X**$^-$ complex in 20 mM Tris, pH 7.4. [**Dye**] = 5 μM, F_0 = fluorescence response of the **Dye** only, F = fluorescence response of the **Dye•X**$^-$ complex where a) is the response of **DSMI•X**$^-$ where **X**$^-$ is NaI, and b) is the response of **DSMI•X**$^-$ where **X**$^-$ is NaCl.

Spectroscopic Analysis

NMR Analysis of AMI•Anion Binding

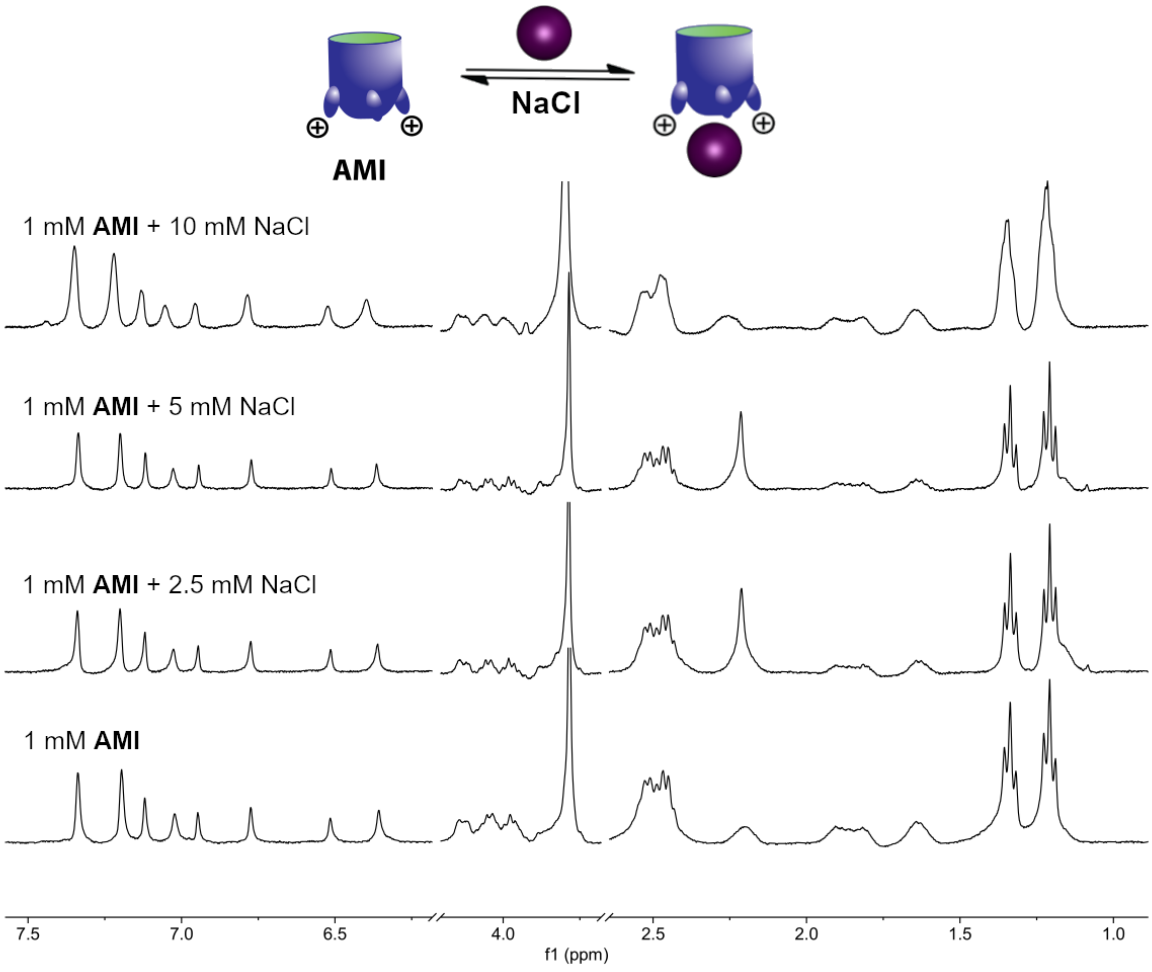

Figure S-15. ^{1}H NMR spectra (600 MHz, D_2O, 298K) showing rapid in and out exchange of NaCl with **AMI**.

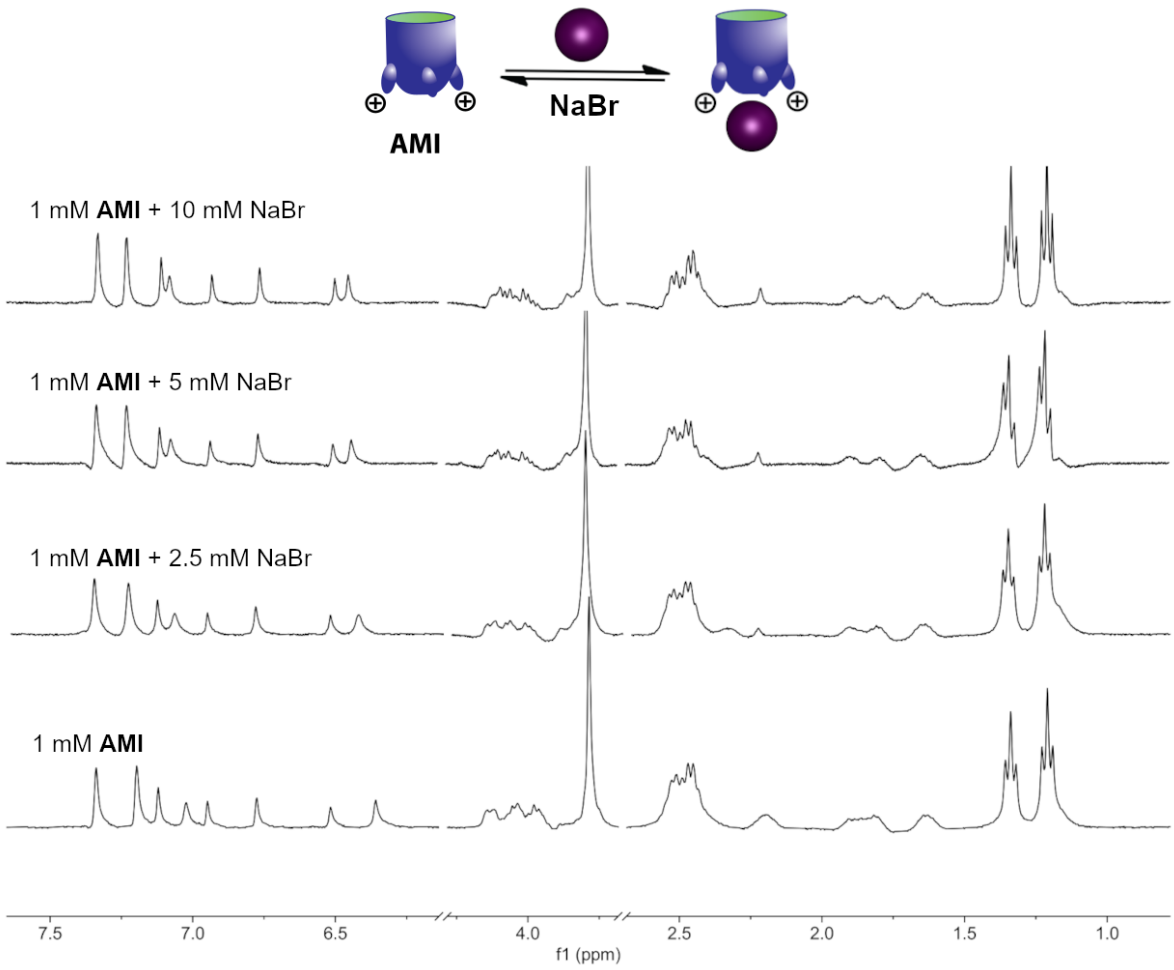

Figure S-16. ^{1}H NMR spectra (600 MHz, D_2O, 298K) showing rapid in and out exchange of NaBr with **AMI**.

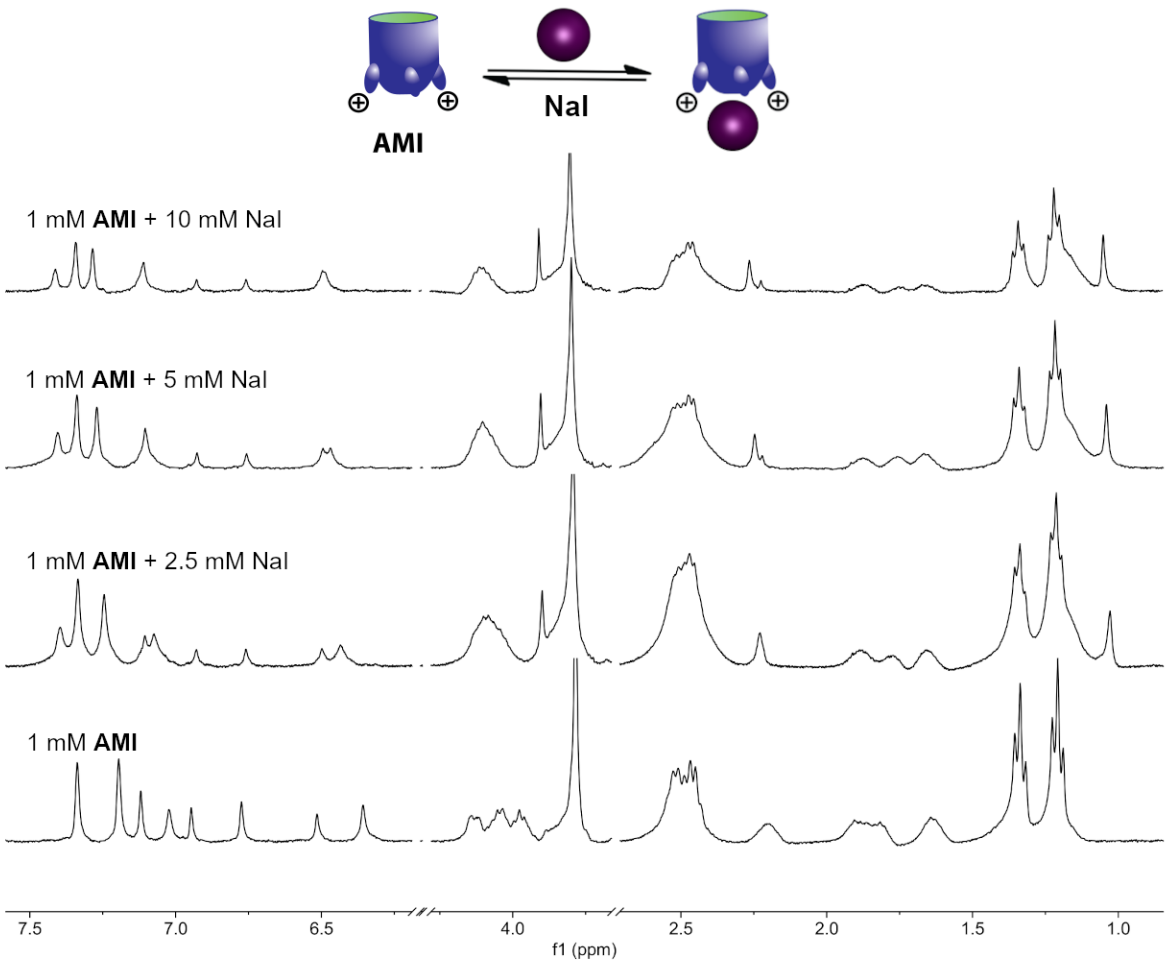

Figure S-17. ^{1}H NMR spectra (600 MHz, D_2O, 298K) showing slow in and out exchange of NaI with **AMI**.

NMR Analysis of AMD•Anion Binding

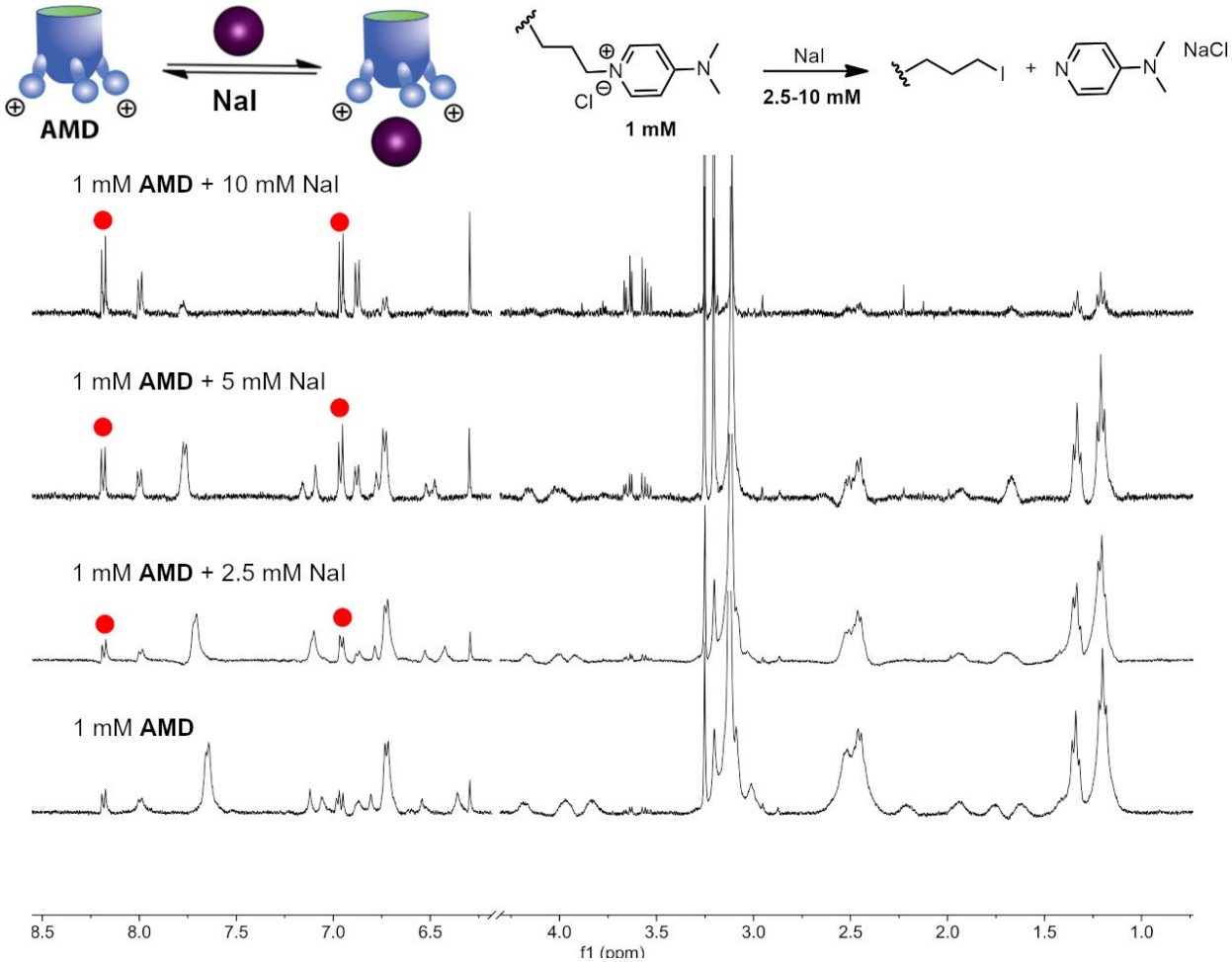

Figure S-18. ^{1}H NMR spectra (600 MHz, D_2O, 298K) titrations of NaI with **AMD** showing cleavage of DMAP groups via substitution reaction with NaI, labeled peaks show emergence of free DMAP as the insoluble AM-Iodide cavitand is formed.

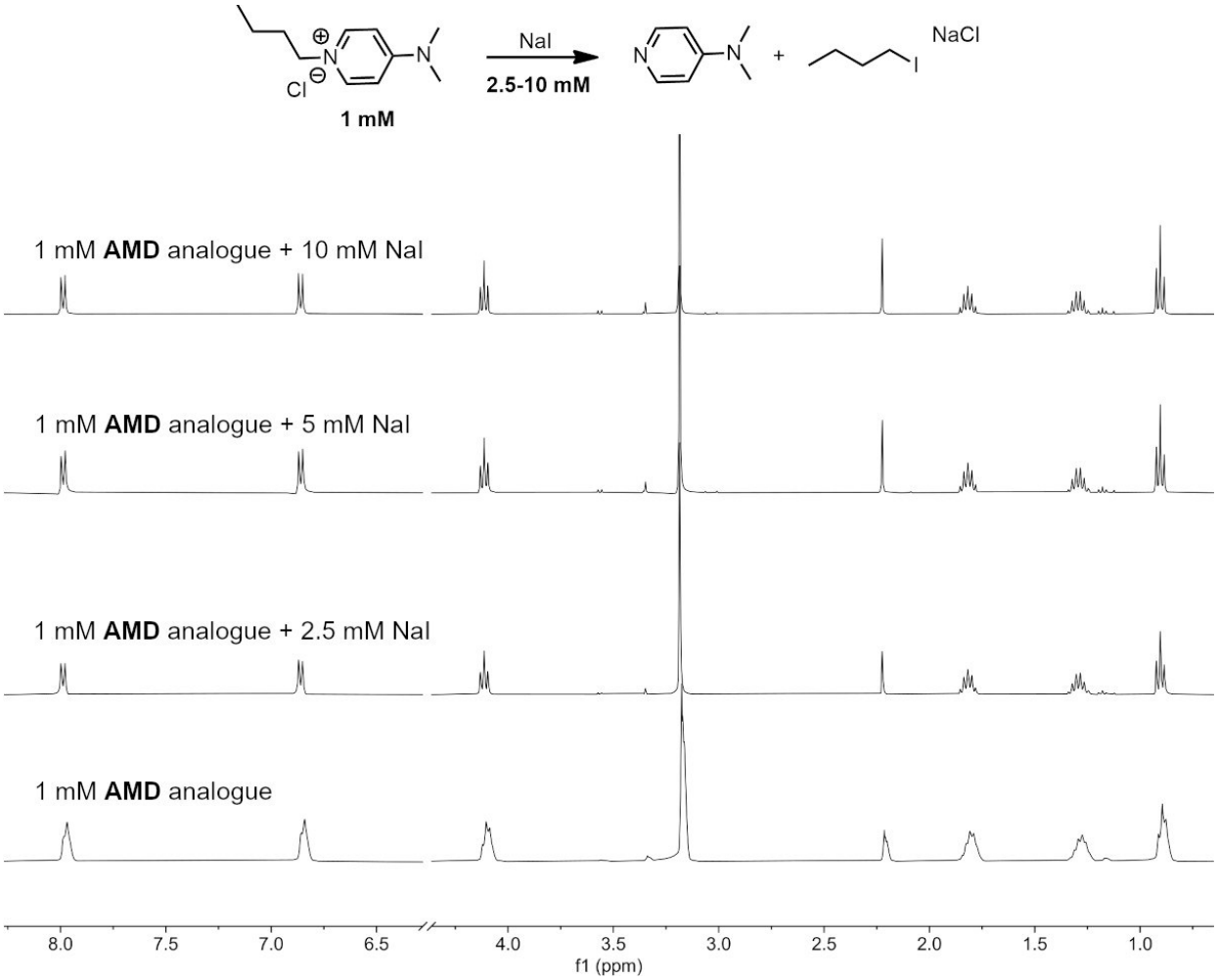

Figure S-19. ^{1}H NMR spectra (600 MHz, D_2O, 298K) titrations of NaI with **AMD analogue** where no substitution reaction with NaI is observed.

Isothermal Calorimetry Analysis of AMI•Anion Complexes

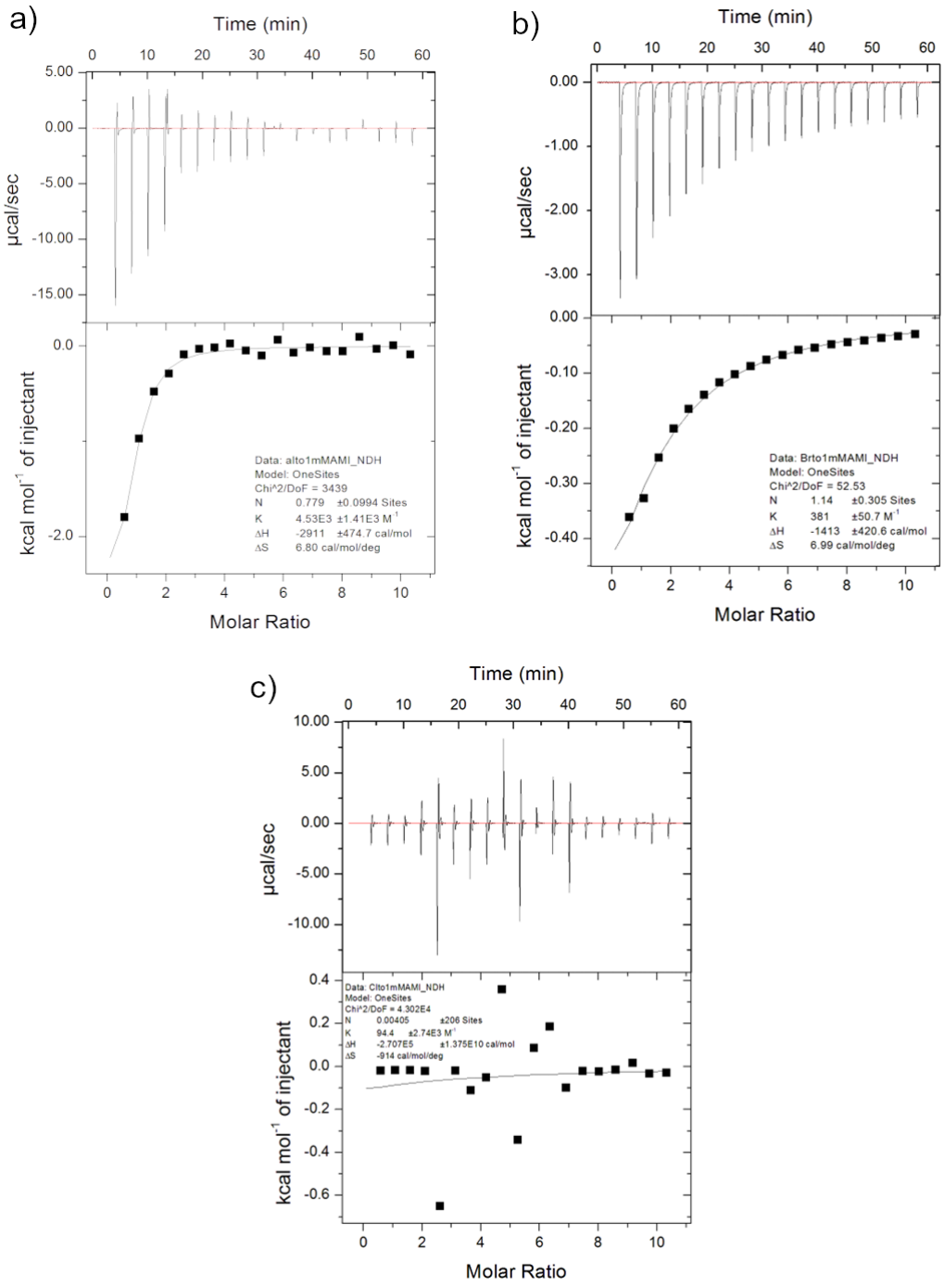

Figure *S-20.* ITC titrations of increasing amounts of a) 50 mM NaI, and b) 50 mM NaBr, and c) 50 mM NaCl with 1 mM **AMI**, measured at 20 °C. The 1 mM **AMI** was placed in the cell and 50mM anion solution in the syringe. All solutions were diluted with ultrapure H_2O. Top trace: raw data for the ITC titration. Bottom trace: binding isotherm of the integrated calorimetric titration data. The heat of dilution, measured by the injection of titrant into H_2O, was subtracted for each titration to obtain the net reaction heat value. ***Note - entry c) shows no binding of Cl^- to AMI.***

Limit of Detection

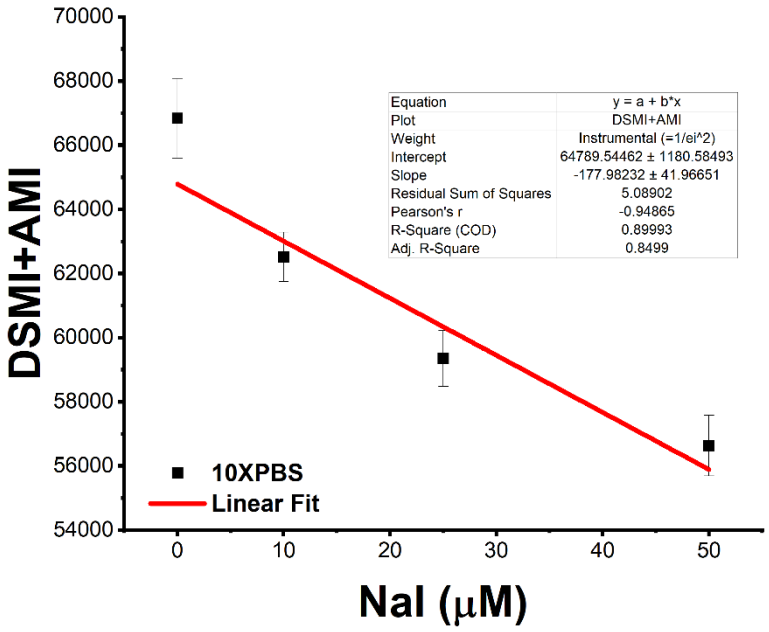

Figure S-21. Limit of Detection (LOD) for **AMI•NaI** complex where [**AMI**] = 5 μM, [**NaI**] = 0-50 μM and [**DSMI**] = 0.5 μM in 10X PBS buffer. Error bars represent the standard deviation of 3 repeats. The calculation was done using the equation *LOD = 3 * (SD of blank) / (slope)* and was found to be 21 μM.

Hill 1 Plots

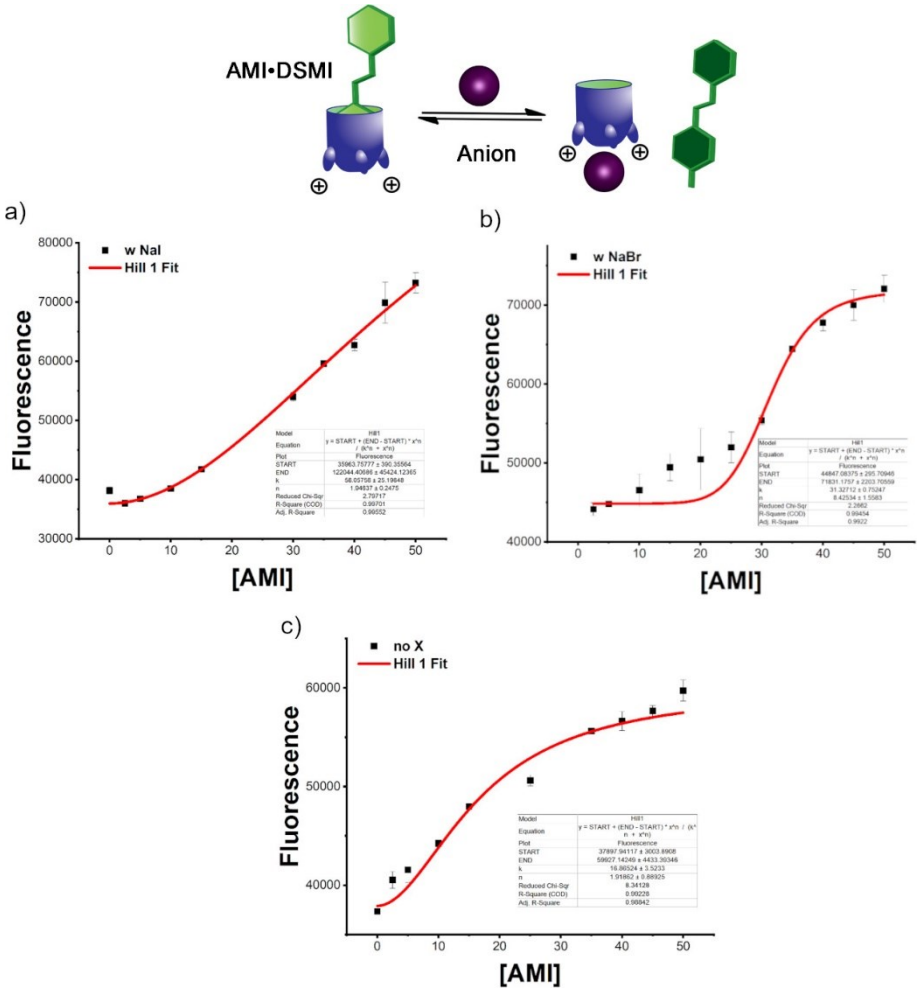

Figure S-22. Hill 1 Plots of **DSMI** with increasing concentration of **AMI**, where a) shows binding with NaI, b) shows binding with NaBr, and c) is a control with no anion. The raw fluorescence of 0.5 μM **DSMI** + 0-50 μM **AMI** with 50 mM NaI, NaBr or no anion in ultrapure H_2O was collected and fitted with Hill 1 equation: *y = START + (END - START) * x^n / (k^n + x^n)* using Origin software. Error bars represent the standard deviation of 3 repeats.

Halide	k	n
No X	16.9 ± 3.5	1.9 ± 0.9
NaI	58.0 ± 25.2	1.9 ± 0.2
NaBr	31.3 ± 0.8	8.4 ± 1.6

Table S-1. Summary of Hill 1 fitting of 0.5 μM **DSMI** + 0-50 μM **AMI** with 50 mM NaI, NaBr, or no anion in ultrapure H_2O.

References

1. A. D. Gill, B. L. Hickey, S. Wang, M. Xue, W. Zhong and R. J. Hooley, *Chem. Commun.* 2019, **55**, 13259–13263.
2. Y. Liu, M. Mettry, A. D. Gill, L. Perez, W. Zhong and R. J. Hooley, *Anal. Chem.* 2017, **89**, 11113–11121.
3. J. Chen, B. L. Hickey, Z. Gao, A. A. P. Raz, R. J. Hooley and W. Zhong, *ACS Sens.*, 2023, **7**, 2164-2169.
4. J. W. Furness, A. D. Kaplan, J. Ning, J. P. Perdew, J. Sun, *J. Phys. Chem. Lett.* 2020, **11**, 8208–8215.
5. S. Grimme, J. Antony, S. Ehrlich, H. Krieg, *J. Chem. Phys.* 2010, **132**, 154104.
6. S. Grimme, S. Ehrlich, L. Goerigk, *J. Comput. Chem.*, 2011, **32**, 1456–1465.
7. F. Weigend, R. Ahlrichs. *Phys. Chem. Chem. Phys.* 2005, **7**, 3297–3305.
8. A. V. Marenich, C. J. Cramer, D. G. Truhlar. *J. Phys. Chem. B.* 2009, **113**, 6378–6396.
9. F. Neese, *WIREs Comput. Mol.Sci.* 2002, **12**, e1606.